UNIVERSITÀ
DEGLI STUDI
DI PADOVA

Sede Amministrativa: Università degli Studi di Padova
Dipartimento di Medicina Molecolare

CORSO DI DOTTORATO DI RICERCA IN: BIOMEDICINA
CURRICULUM : MEDICINA RIGENERATIVA
CICLO: XXIX

Post-translational mechanisms regulating Glutathione Peroxidase 4

Coordinatore: Ch.mo Prof. Stefano Piccolo
Supervisore: Ch.ma Prof.ssa Matilde Maiorino
Co-Supervisore: Dott.ssa Valentina Bosello Travain

Dottorando : Lucia La Pira

Table of contents

ABSTRACT

Glutathione peroxidase 4 (GPx4) is a selenocysteine-containing homolog of the vertebrate glutathione peroxidase family, peculiarly reducing membrane hydroperoxide by glutathione (GSH). GPx4 was first purified in 1982 as a 'peroxidation inhibiting protein', and is emerging to date, together with its substrate GSH, as a major determinant in regulating cell balance between proliferation and death. Recently, it emerged that GPx4 inactivation or GSH depletion in cells causes death by a novel subroutine relying on lipid peroxidation, named ferroptosis. Consistently, reverse genetics studies indicate that all the tissues where GPx4 is in so far silenced undergo degeneration. Understanding therefore GPx4 turnover is a crucial issue.

Major aim of this work was therefore clarifying whether GPx4 could be a Nedd4 substrate, and thus proteasomal degradation could have a role in GPx4 turnover.

This hypothesis was suggested by the presence of a conserved LPXY motif observed *in silico* at the C-terminal end of GPx4, a canonic position typical of many substrates of the WW domains-containing E3 ligases of the Nedd4 family.
In Nedd4.1/Nedd4.2 and GPx4 co-transfected cells, the Nedd4 isoforms are co-immunoprecipitated by GPx4, while mutation at the conserved C-terminal LPXY motif on GPx4, yields a decreased signal of the Nedd4 band, suggesting that the binding between GPx4 and the two Nedd4 isoforms relies indeed on the LPXY motif. Ubiquitylation is observed in co-transfected cells immunoprecipitated as above, but the ubiquitylation pattern is not affected when an inactive mutant of the catalytic Cys of Nedd4.1 or Nedd4.2 is co-transfected with GPx4. Purified rat GPx4 is not ubiquitylated in an *in vitro* assay containing home made recombinant Nedd4.1, E1, E2, ATP and ubiquitin (Ub). Furthermore, overexpressed Nedd4.1 fails to accelerate endogenous GPx4 clearance following a ferroptotic signal, such as GSH depletion or GPx4 modification by the ferroptosis-inducing compound 1S,3R RSL3. In the GSH depletion model, however, GPx4 protein and activity

decreases in the cytosol, while, surprisingly, it appears in the pellet, containing the membrane fraction, in a non-ubiquitylated form. Dissociation constant measurement by SPR analysis on model liposomes interacting with purified GPx4 indicates a decrease in the absence of GSH, while a combined docking and molecular dynamic approach shows that GPx4 binds to the polar head of membrane phospholipid by its basic zone adjacent to the catalytic site. Furthermore, upon oxidation, GSH releases the enzyme in the cytosol by interacting with some residues of the basic zone involved in phospholipid binding. Thus our work, although showing a LPXY motif-dependent binding between both the Nedd4 isoforms and GPx4, fails to validate the hypothesis that GPx4 is ubiquitylated by these ligases, which appear indeed not involved in GPx4 turnover. Yet, the observation that GPx4 translocates to membrane under GSH depletion opens interesting perspectives in the understanding of the mechanism underlying the action of GPx4 on biological membranes.

RIASSUNTO

La Glutatione Perossidasi 4 (GPx4) è un omologo dei vertebrati delle glutation perossidasi. La selenocisteina nel sito catalitico è l'amminoacido redox-attivo, implicato nella riduzione degli idroperossidi di membrana a spese del glutatione (GSH). La GPx4 fu per la prima volta purificata nel 1982, come 'proteina inibente la perossidazione' e ad oggi sta emergendo, insieme al suo substrato GSH, come un elemento determinante nel regolare l'equilibrio tra proliferazione e morte cellulare. Infatti risultati recenti indicano che l'inattivazione della GPx4 o la deplezione di GSH causa morte cellulare attraverso un nuovo meccanismo programmato basato sulla perossidazione lipidica, chiamato ferroptosi. Studi di genetica inversa indicano che tutti i tessuti dove la GPx4 è silenziata, subiscono degenerazione. La comprensione, perciò, dei meccanismi che sottendono il ricambio (turn-over) della GPx4 appaiono cruciali.

Il principale obiettivo del lavoro è stato quelle chiarire se la GPx4 potrebbe essere un substrato di Nedd4, e se la degradazione proteosomale potrebbe avere un ruolo nel ricambio del selenoenzima.

Questa ipotesi è stata suggerita dalla presenza di un motivo strettamente conservato LPXY, osservato *in silico* all'estremità C-terminale della GPx4. Questo motivo infatti è noto per essere riconosciuto dai domini WW contenuto nelle E3-ligasi della famiglia delle Nedd4 ed è presente in molte proteine che sono substrato di Nedd4.

Nelle cellule co-trasfettate con Nedd4.1/Nedd4.2 e GPx4, l'isoforma di Nedd4 co-immunoprecipita con la GPx4, mentre la mutazione del motivo C-terminale LPXY della GPx4, provoca un decremento del segnale della banda di Nedd4, suggerendo che il legame tra la GPx4 e le due isoforme di Nedd4 dipenda dal motivo LPXY. Si osserva anche ubiquitinazione nelle cellule co-trasfettate e immunoprecipitate come sopra, ma il 'pattern' di ubiquitinazione non è influenzato se un mutante inattivo della cisteina catalitica di Nedd4.1 o Nedd4.2 è co-trasfettato con la GPx4. Inoltre la GPx4 di ratto purificata non è ubiquitinata in un saggio di ubiquitinazione *in vitro* contenente la Nedd4.1, gli enzimi E1 e E2, ATP e ubiquitina (Ub). Inoltre, la sovra espressione di Nedd4.1 non induce

un'accelerazione del ricambio della perossidasi, sia quando le cellule non sono trattate che a seguito di uno stimolo ferroptotico, come la deplezione di GSH o l'alchilazione di GPx4 tramite 1S,3R-RSL3. Nel modello di deplezione del GSH, comunque, la proteina GPx4 e la sua attività subiscono una riduzione nel citoplasma, mentre sorprendentemente, la proteina appare nel 'pellet', che contiene la frazione delle membrane in forma non ubiquitinata. La costante di dissociazione dell'interazione di GPx4 e di liposomi contenenti tetraoleilcardiolipina (TOCL), misurato con la tecnica Surface Plasmon Resonance (SPR) diminuisce in assenza di GSH. Inoltre un approccio combinato di docking e dinamica molecolare indica che la GPx4 si lega alle teste polari dei fosfolipidi di membrana attraverso un' area basica adiacente al sito catalitico. Inoltre, dopo ossidazione della GPx4, il GSH rilascia la perossidasi nel citoplasma mediante interazione con alcuni residui della area basica coinvolta nel legame con i fosfolipidi.

In conclusione il nostro lavoro dimostra un legame tra entrambe le isoforme di Nedd4 e la GPx4 che dipende dal motivo LPXY, ma non valida l'ipotesi iniziale che la GPx4 possa essere ubiquitinata da queste ligasi, che quindi non sembrerebbero essere coinvolte nel ricambio della proteina GPx4. Tuttavia, l'osservazione che la GPx4 trasloca nelle membrane in condizioni di deplezione di GSH apre interessanti prospettive nella comprensione dei meccanismi che sottendono l'interazione della GPx4 con le membrane biologiche.

1. INTRODUCTION

1.1 History of a discovery: from PIP to GPx4

Lipid peroxidation was described in 1963 by Hochstein and Ernster (1) and it was appreciated as a detrimental reaction leading to cell membrane destruction. The fact that the reaction required reactants at physiological concentration, namely a reductant, such as NADPH, and an Fe^{3+} chelate, highlighted the possible physiological relevance . In 1976 McCay et al. (2,3) reported that, a GSH-dependent thermolabile 'factor', preventing lipid peroxidation, was present in rat liver extracts. At that time, many groups were concerned about the identity of this factor, but the result of many studies turned out incorrect, since the attention was mainly polarized on either the classical tetrameric glutathione peroxidase (today known as GPx1, E.C. 1.11.1.9) or the dimeric glutathione transferases, both enzymes already known for their glutathione peroxidase activity on small, soluble hydroperoxides (2).

Eventually, the factor purification and characterization was accomplished at the Department of Biological Chemistry of the University of Padua, and published in 1982(4). In agreement with the described function, the newly identified protein was named PIP (peroxidation inhibiting protein). Indeed purified PIP from rat liver could inhibit lipid peroxidation both in liposomes in the presence of vitamin E, or in membranes. Peculiar features of the newly discovered protein were its monomeric nature and glutathione peroxidase activity on fatty acids hydroperoxides esterified in phosphatidyl choline. Later, it was shown that purified PIP contained one gr atom of Se per protein monomer, and that could reduce phospholipid hydroperoxide by a uni-ter ping pong mechanism similar to that described for the classical tetrameric glutathione peroxidase. To underline the enzymatic role, in 1984 PIP was, indeed, renamed 'Phospholipid Hydroperoxide Glutathione Peroxidase' (PHGPx) (5). Later, it was shown that PHGPx could reduce, beside phosphatidylcholine hydroperoxide, cholesterol and cholesterol ester hydroperoxides inserted in membranes and lipoproteins, and that this reaction was not shared with any of the known peroxidases (6,7) .

These, indeed, could only act on fatty acids hydroperoxides hydrolized from phospholipid hydroperoxides by a phospholipase A2 activity and not at all with cholesterol and cholesterol esters hydroperoxides.

In 1991 the primary sequence of PHGPx was partially elucidated by a combined approach of sequencing peptides obtained from the pig heart-purified peroxidase, and of sequencing corresponding cDNA fragments, which were obtained by screening a cDNA library from pig heart by degenerated probes (8). By this approach approximately 75% of the total GPx4 sequence was covered. Interestingly, covered sequence comprised the in frame TGA codon, coding for selenocysteine, as known for other selenoproteins, an observation that unequivocally confirmed the selenoperoxidase nature of PHGPx. At a molecular level, the new peroxidase resulted homologous, but poorly related, to classical tetrameric glutathione peroxidase, although, besides some clusters of more pronounced similarity, the peptide loops composing the active site of the classical enzyme, were remarkably conserved. Three years later, the complete sequence of PHGPx was obtained by whole gene sequence (9). It was found that gaps in the PHGPx sequence corresponded to subunit interaction sites in the tetrameric GPx, which highlighted the peculiar monomeric nature of PHGPx(Fig. 1). Furthermore, gene sequence analysis unequivocally showed that PHGPx was a distinct gene from that of the tetrameric GPx, thus, unequivocally establishing that the two enzymes arise from two distinct genes. In contrast to the gene encoding for tetrameric GPx, that contained only two exons, the PHGPx encoding gene proved to be composed of seven exons. Sec was encoded by an in frame UGA, and the 3'UTR features in the PHGPx gene showed a limited consensus with that of the mammalian selenoprotein gene identified at the time, namely classical tetrameric glutathione peroxidase and 5' deiodinase.

In conclusion PHGPx was the second glutathione peroxidase identified at protein and gene level. However, this was not taken into account when the nomenclature of the growing mammalian homologs of glutathione peroxidases was ordered and PHGPx (E.C.1.11.1.12) was sistematically filed as the *GPx4* gene product (10).

A

```
hsGPx4          MCASR--DDWRCARSMHEFSAKDIDG-HMVNLDKYRGFVCIVTNVASQUGKTEVNYTQLV 57
hsGPx1          MCAARLAAAAAAAQSVYAFSARPLAGGEPVSLGSLRGKVLLIENVASLUGTTVRDYTQMN 60
                ***:*       *:*:: ***: : *   * *   ** * :: **** ** *  :***:
hsGPx4          DLHARYAECGLRILAFPCNQFGKQEPGSNEEIK------EFAAGYNVKFDMFSKICVNGD 111
hsGPx1          ELQRRLGPRGLVVLGFPCNQFGHQENAKNEEILNSLKYVRPGGGFEPNFMLFEKCEVNGA 120
                :*: *    ** :* *******:**   ****           *:: :* :* *  ***
hsGPx4          DAHPLWKWMKIQPKGKG-----------------ILGNAIKWNFTKFLIDKNGCVVKRYG 154
hsGPx1          GAHPLFAFLREALPAPSDDATALMTDPKLITWSPVCRNDVAWNFEKFLVGPDGVPLRRYS 180
                 ****: :::                        :  * : *** ***:  :*  ::**
hsGPx4          PMEEPLVIEKDLPHYF------- 170
hsGPx1          RRFQTIDIEPDIEALLSQGPSCA 203
                   : : ** *:   :
```

B

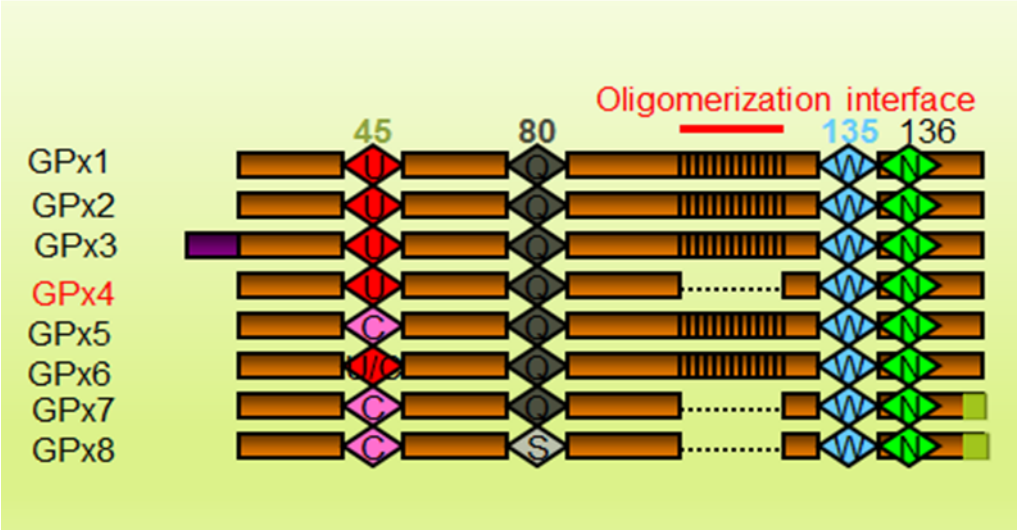

Figure 1. Alignment of human GPx4 and GPx1, sequence (A) and schematic of the vertebrate GPx4 sequence (B). In green, the amino acids of catalytic tetrad are underlined, the asterisk (*) evidences unchanged amino acids and the double point (:) indicates the amino acid with similar property. (B) Conserved feature, among the vertebrate GPx sequences. Residue composing the catalytic tetrad and tetrameric interfaces are indicated. Numbers refer to the human sequence, excluding the initial Met.

1.2 Substrate specificity

Differently from the other glutathione peroxidases (GPxs) that only react with small hydroperoxides (ROOH), GPx4 lacks specificity toward the oxidizing substrate (Fig. 2). Either small ROOHs, such as H_2O_2, that are substrates of the

other GPxs, or more complex ones, such as the hydroperoxide of all the phospholipid classes (PLOOH), including the hydroperoxide in the fatty acids esterified to phosphatidylcholine, phosphatidyletanolamine, phosphatidylserine, cardiolipine or those of cholesterol and cholesterol esters, are good substrates for GPx4 (3,6,11). A possible explanation for this peculiarity relies on the fact that similarly to the other GPxs, GPx4 active site lays on a flat depression on the protein surface, but, peculiarly, the loops contributing to the tetrameric interface in the tetrameric GPxs, are absent in the monomeric GPx4 (Fig. 1B and 3C). This makes GPx4 active site easily accessible to large substrates (Fig. 3A-B). It is likely therefore that the formation of tetrameric peroxidases, which is indeed a late achievement in the evolution (12), allowed the advantage of independently control ROOH content in membrane or in water phases.

GPx4 also lacks specificity for the substrate used as the electron donor for regenerate the active, reduced form of the enzyme. Indeed, it can be reduced by several structurally unrelated low-molecular-weight thiols and specific vicinal or adjacent protein thiols when the GSH concentration becomes limiting. Adjacent (or vicinal) protein thiol oxidation by GPx4 is indeed a critical redox event during sperm maturation (13) . Typically however CXXC proteins like thioredoxins (Trx) or protein disulphyde isomerases (PDI) do not reduce oxidized GPx4 (14).

Enzyme	Oxidizing substrate	K_{+1} (M^{-1} s^{-1})
Bovine GPx-1	H_2O_2	4.5×10^7
	PCOOH	inactive
Human GPx-3	H_2O_2	4×10^7
	PCOOH	inactive
Porcine GPx-4	H_2O_2	1.8×10^6
	PCOOH	1.4×10^7

Figure 2. Substrate specificity of glutathione peroxidases. The substrate specificity of GPx1, GPx3 and GPx4 is reported as rate constant (K_{+1}) for the interaction between the reduced enzyme and the indicated substrate. H_2O_2, hydrogen peroxide; PCOOH, phosphatidylcholine hydroperoxide.

1.3 GPx4 protein structure

GPx1 was the first to be crystallized, and, interestingly, at that time its primary structure was deduced from analysis of the crystal (15). GPx4 was sequenced firstly as a protein and/or cDNA (see above) and initially modeled on the known crystal structure of GPx1. This model indeed was in good agreement with the real crystal structure of GPx4, which became available later.

As mentioned before, being a monomeric protein, GPx4 lacks the quaternary level of protein structure. At the tertiary structure level, GPx4 bears the thioredoxin fold shared with Trxs, glutaredoxins, glutathione S-transferases and Dsba (16), which, from a functional point of view, do not share any specific function, although all of them belong all to the first enzymatic class of the official enzyme nomenclature, i.e. oxidoreductases.

The thioredoxin fold is a distinct structural alpha/beta motif made of four stranded beta sheet and three flanking alpha helices (Fig. 3A), first observed in the *E. coli* Trx, that yield a two layers α/β/α sandwich with a $\beta_1\alpha_1\beta_2\alpha_2\beta_3\beta_4\alpha_3$ secondary structure pattern. In GPx4 and in the other GPxs, the thioredoxin fold contains elements that are not present in Trx: i) two additional beta sheets are located at the N-terminus, ii) one alpha helix and one beta sheet between β_2 and α_2. An additional stretch of aminoacids, located between α_2 and β_3 participating to the tetrameric interface in GPx1 and in the other tetrameric GPxs, which is deleted in GPx4 (Fig. 3A). Since this stretch of aminoacids partially shields the active site Trp residue (see below), it is believed that its absence facilitates accessibility to complex lipid substrates in GPx4.

A typical feature of Trx-like fold is a conserved Cys-X-X-Cys active site motif that is incorporated in the alpha 1 helix, which, interestingly, in GPx4 and in the majority of Sec-containing GPxs is changed into Sec -X-X-Thr. Interestingly, this is located in the α_1 helix, as in Trx. The strongly conserved Thr residue is believed to confer structural stability.

The active site pocket of all the GPx homologs lies in a flat cleft of the protein surface (Fig. 3C) (17). The redox active Se is at hydrogen-bonding distances from three strongly conserved residues, that proved to contribute to catalysis: a Gln, Trp and Asn, located in distant loops in the primary structure (18)(Fig. 3C).

Both in human GPx1 and GPx4, the redox active Se protrudes from a flat area made up by some hydrophobic and basic residues, lending a cationic character to the active site (19). Analysis of the human GPx4 structure shows that, besides the positive charges in close proximity to the peroxidatic Sec, a second large positively charged area is present. In the tetrameric congeners this part is extensively covered by the loop that forms the oligomerization interface. This second cluster of positive charges is expected to contribute to the binding of exposed polar heads of phospholipids, conferring to GPx4 the ability to bind membrane phospholipid and participate to interfacial reactions (19).

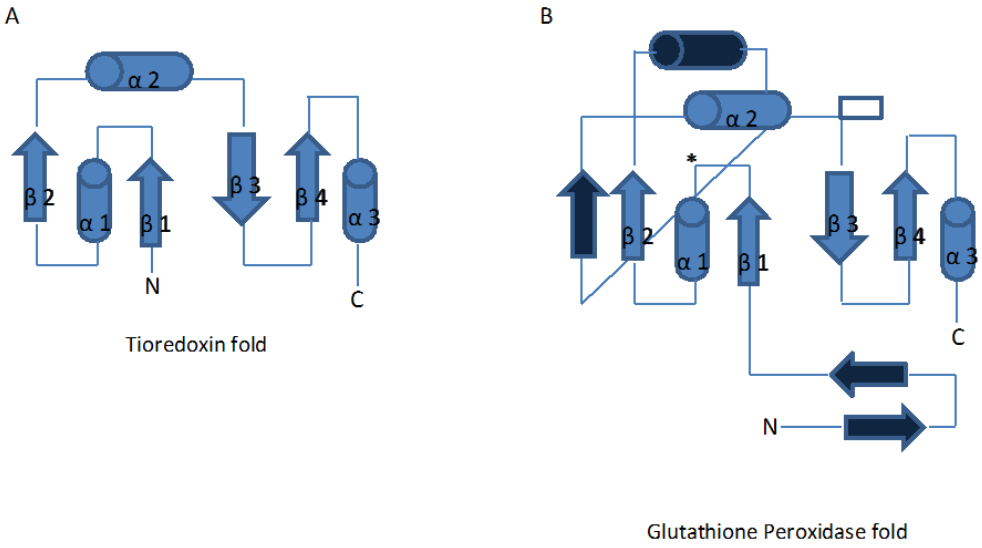

C

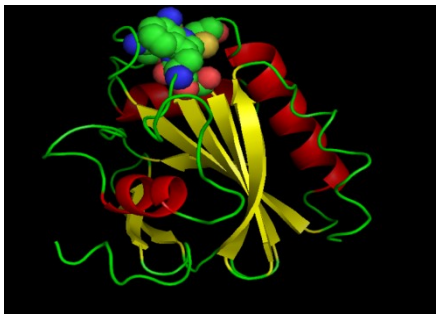

Figure 3. A) The Trx fold and the GPx4 fold compared as tertiary structure. In the GPx fold the asterisk denotes presence of Sec, which corresponds, in homologous position to the N terminal Cys of the CXXC motif of thioredoxins (see text for details).

B) Model of GPx4. Alpha helices are represented in red ribbons, beta sheet in yellow ribbons. The aminoacis composing the catalytic tetrad in balls. The yellow ball is the Sec moiety. Blue ball are nitrogens, and red balls oxygen. Green balls denote carbons

1.4 GPx4 kinetic and catalytic mechanism

The reaction catalyzed by glutathione peroxidases encompasses two independent events: oxidation of the reduced enzyme by a hydroperoxide (ROOH) and reduction of the oxidized enzyme by GSH (17,20) (Fig. 4).

GPx4 was found to follow the kinetic pattern previously described for GPx1, regardless of the distinct substrate specificity. This comply with the observation that the catalytic pocket of the two peroxidases and of the other members of the SeGPx family, which indeed exhibit the same kinetic behaviour of GPx1 and GPx4, is identical. Steady state kinetic analysis suggests a uni-ter ping pong mechanism, where the enzyme is first modified (i.e. the Sec selenol becomes oxidized) by the ROOH, being reduced into the corresponding alcohol, and then reduced back by GSH, (i.e. the oxidized selenium is reduced back to selenol) (Fig. 4). Reduction of the oxidized selenium proceeds by two subsequent steps, the first yielding the glutathionylated enzyme, i.e a selenodisulfide. In the second reduction step a second GSH molecule forms the stable end product GSSG and releases the reduced selenium for the next cycle. In agreement with an accessible and reactive catalytic moiety acid, V_{max} and K_m values are infinite, suggesting that the redox transitions occurring in SecGPx catalytic pocket, are faster than the formation of a typical enzyme-substrate complex and release of products. Thus, even if an enzyme-substrate-complex maybe invoked at least for each of the two reductive steps (Fig. 4), its decay is not rate limiting. In summary, the kinetics of GPxs is similar to that of a chemical catalyst and does not comply with the Michaelis–Menten assumption, where the decay of an enzyme-substrate complex is the rate-limiting step and leads to a saturation kinetics.

The pertinent Dalziel equation that describes this kinetic behavior is the following:

$$[E_0] / v_0 = 1 / k'_{+1} \cdot [ROOH] + 1 / k'_{+2} \cdot [GSH]$$

where k'_{+1} and k'_{+2} are the apparent rate constants for the net forward oxidative and reductive part of the catalytic cycle, respectively (F-G in the Fig. 4).

For the Sec-containing GPxs homologues the apparent rate constant for the oxidizing step (k_{+1}) is among the fastest ever determined for bimolecular enzymatic reactions (around 10^8 M^{-1} s^{-1}). On the other hand the reductive part of the catalytic cycle is the rate-limiting step of the overall reaction as indicated by a lower measured k_{+2} value.

The catalytic cycle of GPx4 as a prototype of the other Sec-containing GPx, which bear the same stable cluster of aminoacids utilized for calculation, was recently studied using a quantum chemistry approach based on density functional theory (DFT) methods (21). This computational mechanistic investigation explored the potential energy surface of the system and the intermediates and transition states of the reaction energy profile. It indicated that, during the oxidative part of the catalytic cycle, a charge separated intermediate is formed by the selenol (F in the Fig. 4), which undergoes deprotonation via long range proton transfer involving the selenol proton, the hydroperoxide, a water molecule and the indole of the Trp residue in the catalytic pocket (see above), leading to the formation of Sec^- and $TrpH^+$. This charge-separated intermediate is greatly destabilized with respect to the reduced ground state enzyme (E-SH, E in the Fig. 4) and it is converted, without appreciable activation energy, to the enzyme form in which Sec is oxidized to selenenic acid (E-SeOH, F in the Fig. 4). Absence of activation energy in this step comply with the elevated k_{+1} value measured by steady state kinetics for the oxidizing step and establish that the selenenic acid derivative of Sec is indeed the oxidized Se form in GPx.

In the reductive step GSH, modeled for simplicity as ethanethiol (Et-SH), forms the selenenylsulfide (or disulfide) intermediate (G in the Fig. 4), which evolves, in the presence of the second molecule of reducing substrate, to regenerate the reduced ground state enzyme E and the oxidized form of the reducing substrate (Et-SS-Et). The second reductive step has the highest activation energy and is thus the rate-limiting reaction of the cycle, which as well agrees with steady state kinetic measurements.

In addition, DFT calculations suggested that absence of reducing substrate leads to an oxidized intermediate which was identified by mass spectrometry as 2 atomic mass units lighter that the reduced, ground form (E-SH).

This intermediate, in the figure named as F', is an eight-membered ring generated by the interaction of selenenic acid with the amide in the backbone, one residue downstream of Sec, forming a selenylamide. Thiolysis of the Se-N bond of the selenenylamide in F' (when the reducing substrate becomes available again) leads to the formation of the mixed Se-disulfide (E-Se-SG, G in the Fig.4), which continues the cycle. The formation of selenylamide seemingly protects SeGPx from inactivation by over-oxidation and/or beta-cleavage leading to dehydroalanine (Dha). Notably, the formation of Dha from the selenylamide can only take place when the structure of the enzyme is disrupted, supporting the conclusion that selenylamide, once formed in the active site, contributes to the stability of the oxidized form when GSH is absent or severely limiting.

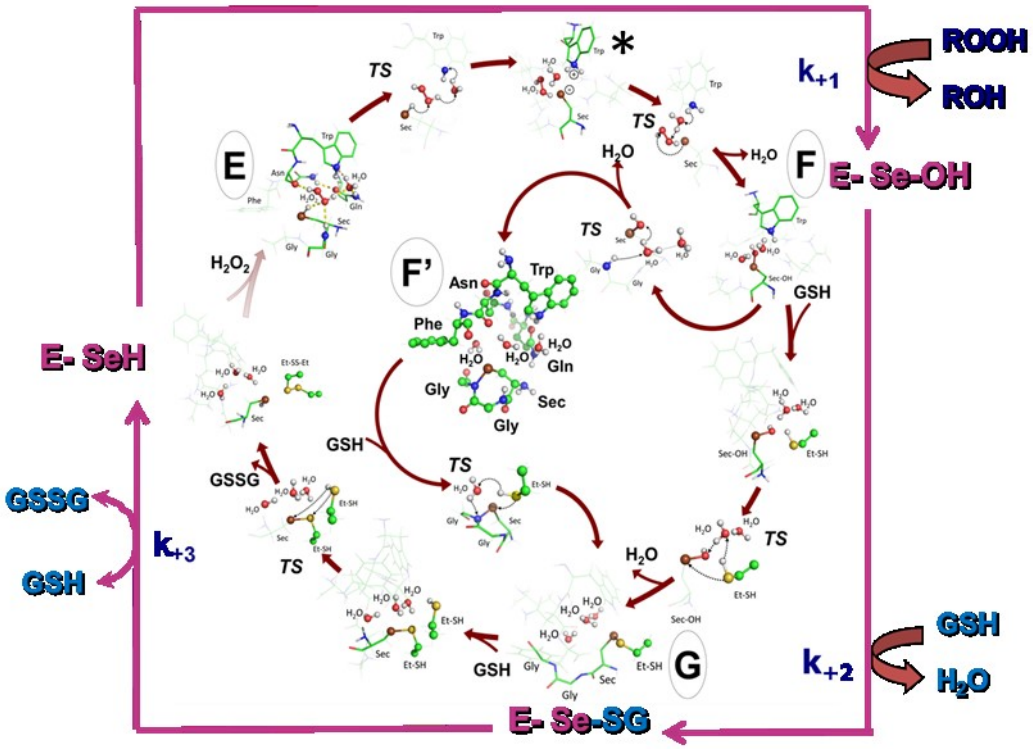

Figure 4. The catalytic mechanism of SecGPx. E-SeH is the reduced enzyme, E-SeOH the oxidized selenenic acid derivative, E-Se-SG the mixed disulphide with GSH. Inside the corresponding structures as suggested by the quantum chemistry approach. The charge separated intermediate is indicated by *. See text for details.

1.5 Functions

GPx4 is needed for life. Apparently embryo development (22), cell survival and thus proliferation (23), inflammation (24,25), and male fertility (26) rely on GPx4. Recent evidence suggests also roles in metabolism and viral infection (27). The most known role in male fertility and cell survival will be described below.

1.5.1 mRNA expression and individual transcript function

After the gene sequence of GPx4 was elucidated, it was appreciated that this enzyme is transcribed into mRNA of different lengths which leads to three different isoforms differing in their N-terminal extension: a cytosolic short form (cGPx) and a mitochondrial long form, containing a mitochondrial leader sequence (mGPx4), arises from alternative usage of two alternative starts located in the first exon, while a nuclear form, which contain a nuclear localization sequence (nGPx4) arises from the alternative transcription of an alternative exon located within the first intron, which is under control of an alternative promoter (28–31) (Fig. 5). Since the mitochondrial leader sequence is cleaved off in the mature protein, mGPx4 and cGPx4 are undistinguishable (31). This led to misinterpretation, because several experiments indicate that the real location of the enzyme not finely described by the location that can be deduced based on the type of transcript produced, particularly for cGPx4. Several studies indeed imply that cGPx4 is also present, beside the cytosol, in the nuclei and in the intermembrane space of mitochondria (32,33).

As mentioned above, GPx4 is needed for life: ablation of the entire gene leads to embryonic lethality at the gastrula level with hallmarks of apoptosis (22).

Some vital mutations yielding truncation of GPx4 have been reported in a rare form of spodylometaphyseal displasia, of previously unknown molecular basis (34) . These highlight the role of GPx4 in embryo development. Spodylometaphyseal dysplasia is a neonatal lethal form of disease characterized by severe metaphyseal chondrodysplasia with mild limb shortening,

platyspondyly, cardiac conduction defects, and central nervous system abnormalities. Two of these mutations were found in an affected child: the first was inherited from the mother, and results in splicing out of part of exon 4, while the second was de novo, and results in skipping of exon 5. A third was found in the two unaffected parents that carry the same heterozygous stop mutation in exon 3 of GPx4, yielding a premature stop in exon 3 . Interestingly, all the three mutations, which are predicted to cause premature termination of GPx4, affect the enzyme downstream of the catalytic Sec, suggesting that catalytic activity is not completely abolished, otherwise mutations would be not compatible with life.

Comparison of the phenotypes obtained from genetic manipulations affecting the distinct mRNA forms arising from *GPx4*, allows conclusive understanding about the physiological role of these products. These can be summarized as follows:

1. cGPx4, which is expressed at relatively low levels in all cell types, is linked to the general vital function of GPx4, both in somatic and immature male germ cell of the testis.

2. mGPx4, which is expressed at high levels in testicular cells only (26), has not a vital function, but a crucial role in male fertility by stabilizing the midpiece of spermatozoa.

3. nGPx4, which is expressed at relatively low levels in testicular cells and even lower in other somatic cells (31), has not a vital function and is not either crucial to male fertility, but it provides stability to nuclear chromatin in maturating spermatozoa.

Indeed, transgenic mice overexpressing cGPx4 over a $GPx4^{+/-}$ background (Tg(cGPx4)$GPx4^{+/-}$), when crossed with wild type $GPx4^{+/-}$ yielded a normal offspring of mice overexpressing cGPx4 over a $GPx4^{-/-}$ background [i.e Tg(cGPx4)$GPx4^{-/-}$] . This demonstrated that the cGPx transgene was able to rescue the lethal phenotype of the GPx4 null mutation (33). The observation that indeed the transgene Tg(mGPx4)$GPx4^{+/-}$ when crossed with wt $GPx4^{+/-}$, failed to produce any Tg(mGPx4)$GPx4^{-/-}$ offspring, undoubtably proves that mGPx4 cannot rescue the lethal phenotype of mice lacking the entire *GPx4*. Interestingly, the

males of the Tg(cGPx4)GPx4$^{-/-}$offspring, similarly to males lacking specifically mGPx4 (26) were infertile although they did not exhibit any defect at the level of the testicular or epidydimal tissue. These mice indeed, that lack mGPx4, exhibit sperm malformations, i.e. bends between the principal piece and the mid piece, similar to those recapitulated by mGPx4$^{-/-}$ mice. Altogether this suggests that mGPx4 is not involved in somatic or male germ, and cell survival. This is indeed the job of cGPx4. Furthermore, it points out once again that it is the lack of mGPx4 that yields sperm malformation.

The above results comply with another independent approach, where the entire GPx4 gene was knocked out specifically in spermatocytes and spermatids but not spermatogonia (the diploid stem cells of the testis) or somatic cells (35). In addition to the sperm defects observed in male mGPx4$^{-/-}$mice (26) and in the Tg(cGPx4)GPx4$^{-/-}$ (33) male mice and, partially in severe selenodeficiency (36), this model yielded an increased cell death of the aploid cells of the germinal epithelium, but not spermatogonia or somatic cells. Together with the observation that the testicular tissue of cGPx4 overexpressing mice (over a GPx4 null background) or that of the mGPx4 null mice has a normal appearance, the loss of spermatocytes and thus spermatids in the above conditional KO model can be ascribed to the absence of cGPx4 expression, thus highlighting the survival role of cGPx4, beside in somatic cells, in haploid male germ cells.

Indeed GPx4 arising from the nuclear transcript, nGPx4 (31), appears involved in sperm chromatin stability. Maturating spermatozoa from nGPx4 KO mice exhibit defective chromatin condensation and an increased ratio of protein thiols/disulfides when compared to wild types, suggesting that nGPx4 has a stabilizing role in the sperm nucleus. The animals are fertile however, thus apparently these defects are not severe enough to impact on fertility (37).

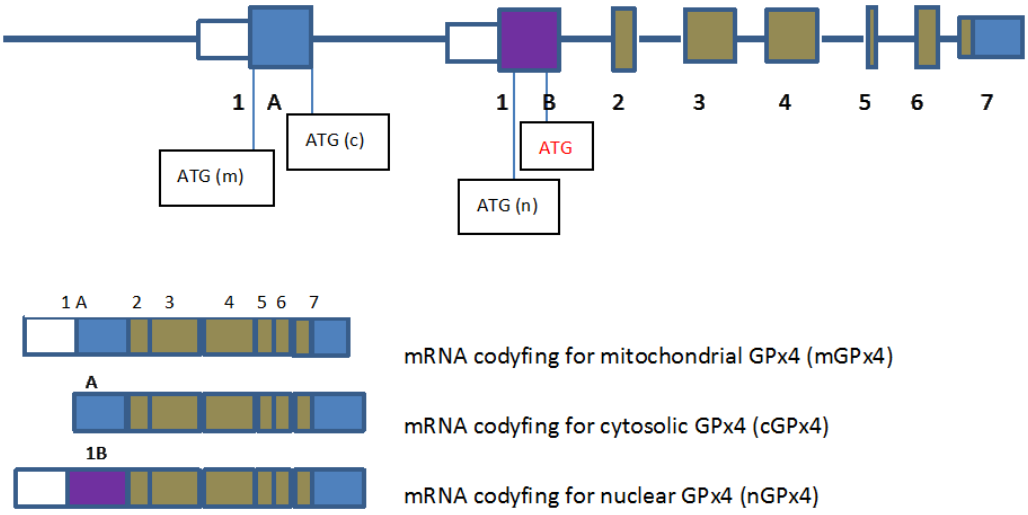

Figure 5. Structure of *gpx-4* gene and its mRNAs. Coloured boxes are representing exons. Exon 1A is allowing the transcription of mitochondrial or cytosolic GPx4 form and instead exon 1B is related to nuclear GPx4 form. 5' UTR of mitochondrial and nuclear transcripts are represented by small white boxes. Translational ATG codon of three protein products is shown. In orange, the second ATG is signed inside the alternative exon of rodents.

1.5.2 Role in male fertility

Starting from 1969, studies on Se-deficient mammals established that Selenium is of pivotal importance for male fertility. In rodents, second generation selenium deficiency results in reduced fertility (mouse) or complete loss of fertility (rats) (36). The seminiferous tubule from the deficient animal contains fewer elongating spermatids and spermatozoa, and releases immature round spermatids into the severely contracted lumen, suggesting that the process of spermatogenesis is disturbed. Furthermore, when spermatogenesis continues, epididymal spermatozoa exhibit lesions at the level of the midpiece. Bends between principal piece and the midpiece are observed, while ultrastructural studies show that the primary abnormality is the shape and the arrengement of

the mitochondria forming the midpiece sheath. In 1999 our group found that, in the midpiece of mature rat spermatozoa, GPx4 represents at least 50 per cent of the sheath that embeds the helix of mitochondria and that, in this location, GPx4 is present as an enzymatically inactive, oxidatively cross-linked insoluble protein. Moonlighting of GPx4 into a structural protein could explain the mechanical instability and the mid piece lesion of Se-deficient sperm (38).

As already pointed out (see paragraph 1.5.1) more recent independent inverse genetics approaches agreed in showing that male fertility requires the contribution of all the three products arising from *GPx4,* with a dispensable contribution only of nGPx4 indeed.

cGPx4 appears mainly related to germ cell survival, and its disturbance might explain the reduced spermatogenesis observed in Se deficient animals. The effect of cGPx4 on survival is connected to reduction of peroxides (i.e. the oxidative part of the catalytic cycle). By preventing lipid peroxidation, GPx4 counteracts cell death (Fig. 6). Therefore the role of the mGPx4 and nGPx4 is related to the moonlighting into a structural component and sperm structural stabilization. This is connected to the reductive part of the catalytic cycle, depending indeed on the limited specificity for the reducing substrate of GPx4. During late spermatogenesis, when glutathione (GSH) levels fall down (39), mitochondrial GPx-4 uses as reducing substrate, in place of GSH, the thiol groups of SMCP and other Cys-rich proteins of the sperm mitochondrial capsules (38). The nature of the GPx4 oxidizing substrate ROOH participating to sperm maturation remains unknown. Such a reaction yields cross-linked protein substrate and cross-linked GPx-4 by S-S or Se-S bridges. In this form GPx4 is enzymatically inactive and promotes stability to the sperm mitochondrial capsule. Nuclear GPx-4 works similarly on chromatin, although the consequences are less dramatic, nGPx4 KO only exhibiting sperm head instability.

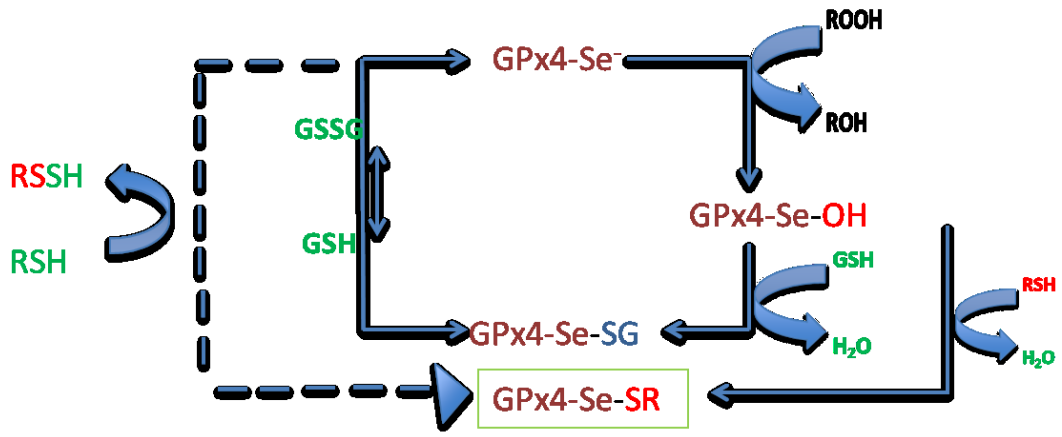

Figure 6. Mechanism of stabilization of the sperm midpiece an nuclear chromatin by GPx4. The internal square represents the usual catalytic cycle, as depicted in figure 4, which takes place in somatic cells. In maturating male germ cells the GSH levels fall down (39). Therefore oxidized GPx4 (GPx4-SeOH) uses protein thiols (RSH) as electron donors, and thus mixed Se-S disulfides between GPx4 and the protein (GPx4 – Se-SR) or disulfides (RSSR) are formed. In the latter case reduced GPx4 (GPx4-Se-) is regenerated for another cycle

Moonlighting of GPx4 into a structural protein could explain the mechanical instability and the mid piece lesion of Se-deficient sperm.

1.5.3 Role in cell survival

GPx4 is essential for life(22). The absence triggers an novel form of cell death called ferroptosis (40). The mechanism underlying is inhibition of lipid peroxidation.

Inhibition of lipid peroxidation

Studies in the '80ties suggest that the peroxidative chain, leading to membrane destruction, results from iron-mediated PLOOH decomposition (41,42).

Lipid hydroperoxides can be formed enzymatically by lipoxygenases (LOXs) or spontaneously upon exposition to air of polyunsaturated fatty acids containing at least one cis,cis-1,4 pentadiene moiety in the presence of traces of iron. LOXs are

abundant in nature and found both in plant and animal cells (43). Mammalian cells contain three different lipoxygenase activity, which are denoted according to the positional specificity of the oxygen insertion into arachidonic acid, i.e. 15-, 12-, 5- lipoxygenase. 15-lipoxygenase is unique among lipoxygenases in its capability to perform lipoxygenation of polyunsaturated fatty acids esterified to phospholipids in biological membranes, a feature that was suggested to relate to the degradation of intracellular membranes (44,45). The relevance of LOX activity in ferroptosis is not clear. Its involvement was initially suggested by the evidence that an inhibitor of 12,15-LOX, rescued GPx4 knock-out cells from lipid peroxidation which preceeds cell death (46). However, LOX depletion could not rescue the death phenotype generated by GPx4 depletion (47) , thus posing some doubts about the involvement of LOX in ferroptosis. More recently, however, it has been shown that, in mouse, male subfertility induced by heterozygous expression of catalytically inactive GPx4 is rescued *in vivo* by systemic inactivation of the Alox15 gene. This suggested that inadequate vitality of germ cells lacking GPx4 is improved by depletion of 12/15 LOX (48), which indeed points for a role of LOX in counteracting survival promoted by GPx4. Pre-formed hydroperoxides are required indeed for LOX activity, presumably because the latter oxidize the LOX non-heme iron at the catalytic site (49)
LOX catalytic activity consists of four simple and controlled steps (50) (Fig. 7),

- Hydrogen abstraction of the methylene carbon in the cis,cis-1,4 pentadiene moiety of a polyunsaturated fatty chain forming a carbon centered radical (L°)
- Radical and doble bond rearrangement, forming a conjugated diene
- Oxygen insertion, forming a conjugated lipid hydroperoxyl radical (LOO°)
- Reduction of the LOO° into LOO- by LOX iron and product dissociation

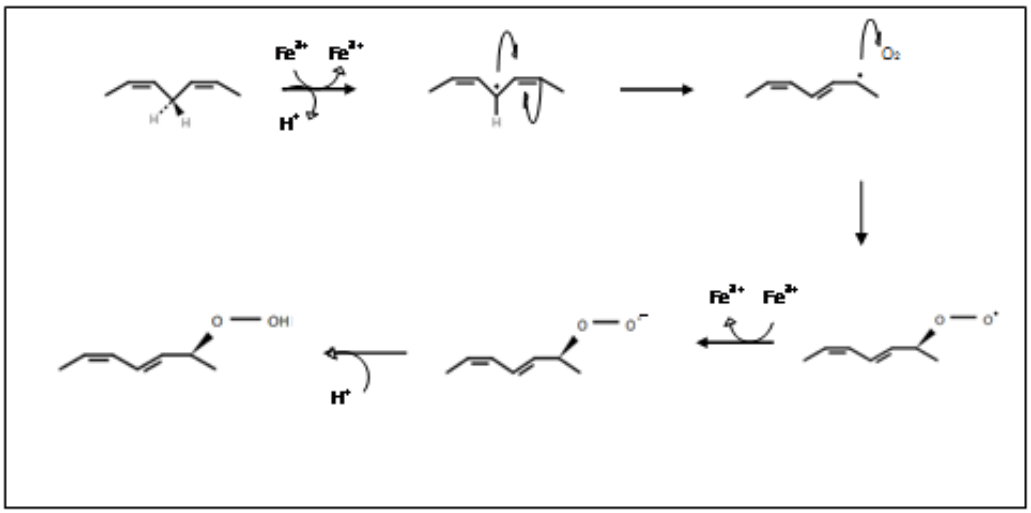

Figure 7. Reaction mechanism of LOX. LOX acting on a cis, cis 1,4 pentadiene is shown.

However, the production lipid hydroperoxides by LOX enzymes is not sufficient to trigger lipid peroxidation and consequently ferroptotic cell death (51). Evidently PLOOH become harmful when are decomposed by reduced iron, a process called 'branching' in lipid peroxidation, that yields, besides new PLOOH, reactive aldehydes, including malondialdehyde, 4-hydroxynonenal (HNE), and truncated fatty acid chains in the membrane phospholipid.

In vitro, GPx4 and GSH, by reducing PLOOH, prevent lipid peroxidation, because, as mentioned above, the initiation of the peroxidative chain reaction requires sparking amounts of preformed PLOOH. Notably, the reduction of LOOH also inactivates LOX, that rely on these compounds for activation (see above). Vitamin E slows down the rate of membrane lipid peroxidation by intercepting the peroxidation-driving lipid hydroperoxyl radicals (PLOO°) (41). In this case, the product of the antioxidant reaction of vitamin E is PLOOH, which may decompose in the presence of Fe^{2+}, and thus, the activity of GPx4 is essential for the antiperoxidant effect of vitamin E. This mechanism, which was proposed based on *in vitro* studies, does not comply with the observation that cell death by GPx4 depletion can be rescued simply by adding vitamin E to the cell culture (43), since the action of vitamin E does not avoid formation of minute amount of PLOOH. One possibility is that vitamin E acts on LOX by reducing back the Fe^{3+} of the active form of the LOX, thus yielding the inactive enzyme.

The practical outcome is that aerobic life continuously produces, by different mechanisms, traces of LOOH, from which enzymatic or non-enzymatic lipid peroxidation may be initiated by ferrous iron complexes or LOX. For this reason, critical event initiating the lipid peroxidation chain reaction seems a missed inhibition rather than an increased initiation rate.

The RAS homologs are a family of oncogenes belonging to the class of small G proteins (52). Being connected to the MAPK/ERK pathway, they are involved in many aspect of cell growth, proliferation and survival. The term RAS derives from Rat Sarcoma virus, where the gene was first identified. There are three Ras genes in humans (HRas, KRas and NRas) that are the most common oncogenes in human cancers. The RAS-phenotype was initially considered to have an important correlation with ferroptosis since it was found that Erastin induced preferentially lethality in HRAS-overexpressing cell lines (53). A possible explanation of the relationship between RAS phenotype and Ferroptosis, seems to be the influence of the oncogene on iron metabolism. However, available data not always agree in this respect. Recently, a study on RAS-mutant in rhabdomyosarcoma cells, evidences instead a resistance to oxidative stress-induced ferroptotic cell death (54). Furthermore oncogenic RAS appears not contributing to sensitivity for Erastin. Thus there is still more to understand about RAS activity and Ferroptosis. However the possibility that cancer cells can be killed by FIN I or FIN II (see below) compounds inducing lipid peroxidation by GPx4 inhibition seems unrealistic. Lipid peroxidation infact requires oxygen, and oxygen is often limiting in poorly vascularized tumors.

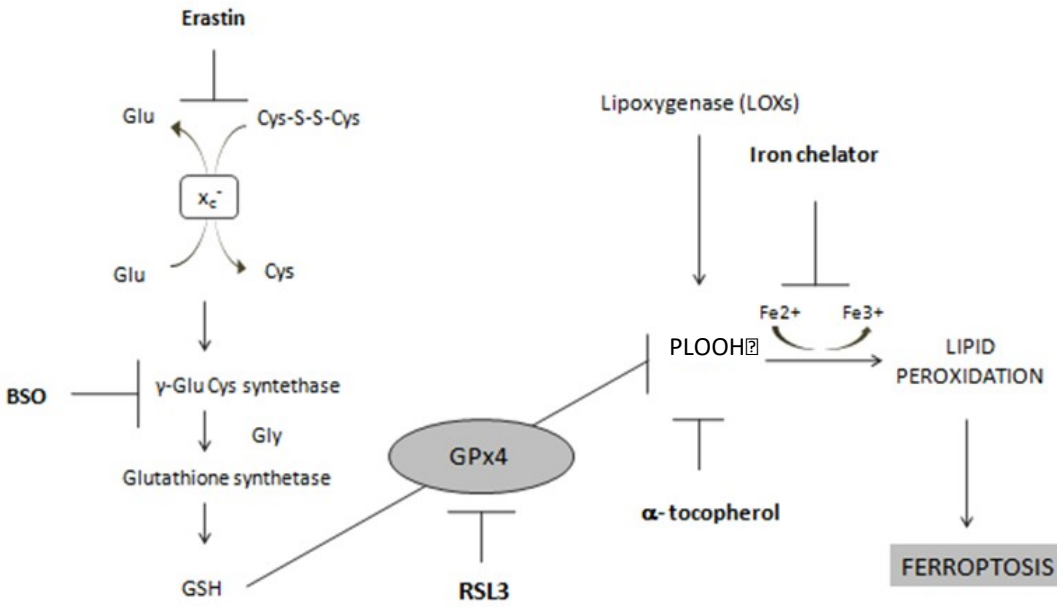

Figure 8. The process of ferroptotic cell death and its pharmacological inhibition. The x_c^- antiporter replenish the cell of Cys for GSH biosynthesis (left). GSH is used as substrate for GPx4 (in the middle) for reducing membrane hydroperoxides (PLOOH), thus preventing cell death by ferroptosis. Erastin (acting on the x_c^- antiporter) and BSO (inhibiting γ-glutamilcysteine synthetase) deplete cells of GSH and therefore antagonize GPx4 function by decreased substrate availability (class I FINs). 1S, 3R- RSL3 directly binds GPx4 (class II FINs). By preventing branching and/or inhibiting LOXs, alpha tocopherol (vitamin E) minimize (or prevent) the amount of PLOOH. Iron chelators, such as Desferoxamine, inhibit the process by chelating free iron.

Pharmacological inactivation of GPx4

GPx4 gene silencing in the mouse leads to cellular degeneration (46,55,56). It appears therefore an appealing target to promote survival or kill cancer cells. This has been attempted by pharmacological inactivation, as discussed below.

Pharmacological inactivation of GPx4 can be triggered by the ferroptosis inducing agents (FINs), which inactivate GPx4 by different mechanisms. FINs have been divided into two classes:

- Class I FINs

Class I FINs cause ferroptosis by depleting the reducing substrate of GPx4, glutathione (57).

Glutathione is one of most important, non-enzymatic antioxidants, ubiquitously expressed in cells and in living organisms in the millimolar range, representing about 80% of low molecular weight thiols (58). It is a tripeptide (γ glutamyl-cysteinyl-glycine), where the Glu is linked to Cys with atypical peptide bond (γ-glutamyl bond) between the γ carbon of the carboxyl-group of Glu and the alpha amino group of Cys, whose alpha carboxylate is in turn linked to Gly by a regular peptide bond (Fig. 9A). The crucial reactive site of GSH is the thiol of the Cys residue. GSH biosynthesis proceeds via two step-reactions, regulated by two ATP-dependent ligases (Fig. 9B).

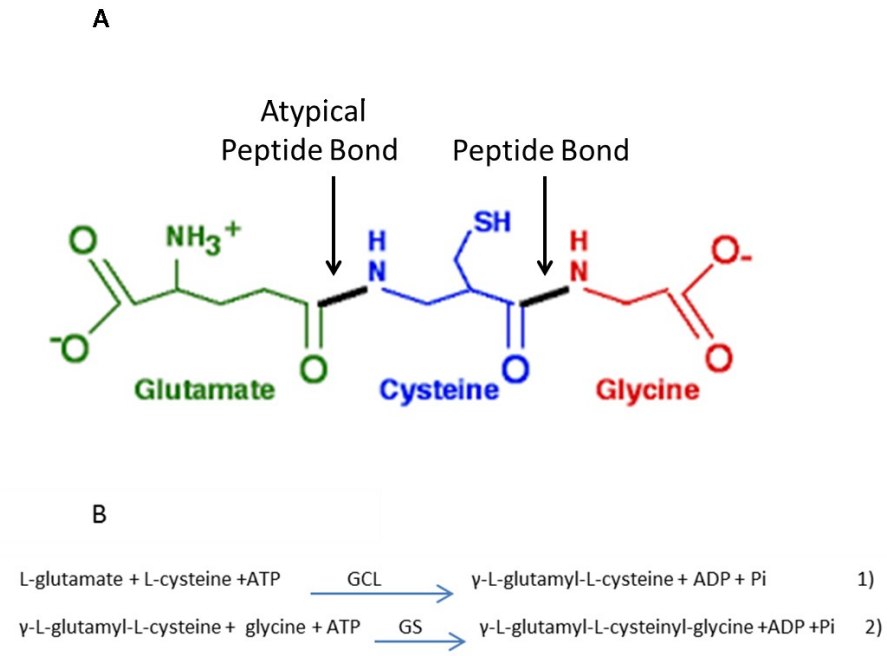

Figure 9. (A) The Glutathione molecule. Composing aminoacids and bonds in reduced glutathione is represented on top. (B) The steps of GSH biosynthesis are represented. In the first step the glutamate-cysteine ligase (GCL), also called γ-glutamilcysteine synthetase (GCS), catalyses the formation of the gamma glutamyl bond between glutamate and cysteine to form γ-glutamilcysteine, using one ATP molecule. In the second step another ATP molecule is used by the glutathione synthetase enzyme (GS), a ligase which adds glycine to γ-glutamilcysteine to synthetize the final product, i.e. glutathione or γ-glutamil-L-cysteinyl-glycine, consuming a second ATP molecule.

Among class I FINs, there is L-Buthionine-S,R-sulfoximine (BSO), which inhibits irreversibly the GCL enzyme, involved in the first step of glutathione synthesis (59).

Another compound, affecting intracellular glutathione content, is erastin. Cellular glutathione depletion by erastin is due to the inhibition of the glutamate/cysteine exchanger x_c^- (60–62) .

x_C^- is an heterodimeric antiporter of plasma membrane, composed of twelve transmembrane transporter protein SLC7A11 (xCT), that are linked to the single transmembrane regulatory protein SLC3A2 (4f2hc) by a disulfide bridge. (Fig. 10) The antiporter is responsible of cystine uptake. Cysteine is a precursor of Cys, one of three amino acids constituting GSH.

While glutamate and glycine are highly available within cells, Cys levels are the rate-limiting factors in the GSH biosynthesis. Cys can be synthetized *ex novo* by the transsulfuration pathway from methionine or can be obtained from the extracellular environment in the form of cystine by the xCT transporter. Cystine is exchanged with intracellular glutamate in an one-to-one ratio by xCT. Once inside the cells, cystine is reduced to Cys and participates to GSH synthesis (Fig. 10)

The mechanism of erastin in inducing ferroptosis relies indeed on a direct inhibition of system x_c^- by binding to the SLC7A11 subunit.

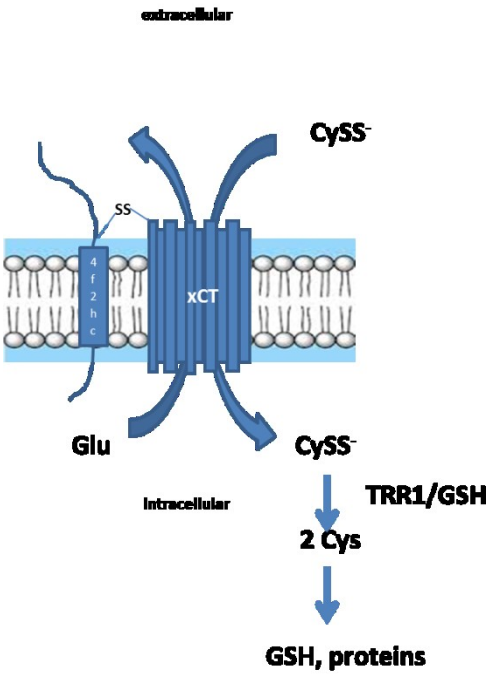

Figure 10. Structure of X_C^- and import of cystine. The cysteine-glutamate antiporter is constituted from 12-transmembrane protein, named SLC7A11. A disulfide bridge links SLC7A11 to SLC3A2 regulatory subunit (4f2hc) . Extracellular Cystine ($CySS^-$) is exchanged for intracellular glutamate (Glu). Once inside, cystine ($CySS^-$) is rapidly reduced by thioredoxin reductase (TRR1) to cysteine (Cys), and in this form is used for GSH and proteins synthesis (63,64) .

Sulfasalazine was found to be a novel, potent inhibitor of the x_C^- transporter (57).

The antiporter x_c^- can also be inhibited by high concentration of extracellular Glutamate (62). In fact, the excess of glutamate is toxic for the cells, just because it doesn't allow the extracellular cystine uptake, affecting the synthesis of GSH. Glutamate toxicity is the main cause of oxidative stress inducing cell death in neuronal cells.

- Class II FINs

Differently from I class FINs, class II FINs directly inactivate GPx4 (57).

It was shown indeed that, in cells, the compound 1S,3R-RSL3, directly targets GPx4(65) binding to it, thus leading to enzyme inactivation. It is hypothesized that this occurs because 1S,3R-RSL3 contains a chloroacetamide electrophile group which reacts with the nucleophile Sec at the active site of GPx4, which was indeed indirectly demonstrated (66). Interestingly, the reaction is stereospecific: only the 1S,3R-RSL_3 isomer is able to induce ferroptosis in sensitive, HRAS overexpressing cells. Western blotting and proteomic analysis on BJeLR cell lysates, treated with 1S,3R-RSL3-fluorescein or 1R,3R-RSL3-fluorescein, indeed revealed that GPx4 is one of the major targets of 1S,3R-RSL3 but not of 1R,3R-RSL3. Other small molecules, such as CIL56 (67) and FIN56 (68), appear to mimic the effect of 1S,3R-RSL3 in inducing ferroptotis.

1.5.4 Role in inflammation

By reducing LOX and cyclooxygenase (COX) activating ROOH, GPx4 dampens inflammation by inhibiting LOX and COX activity (24,25,69,70). However this function is shared with the other GPx, which act on free fatty acids-OOH (FFA-OOH) or H_2O_2. However, a specific involvement of GPx4 has been suggested in some models: i) a conditional knockout (KO) model of GPx4 in neurons, in which mice develop astrocyte inflammation associated with reactive astrogliosis and neurodegeneration (46), suggested a specific anti-inflammatory function of GPx4 in vivo, ii) transformed cells bearing an increased 12/15 LOX activity resulting from GPx4 ablation, which surprisingly survive, once implanted into mice yield increased tumor angiogenesis (71). This suggests that inhibition of eicosanoid production by GPx4 plays a role in biology of cancer progression.

Recent evidence indicates that the control of inflammation linked to the regulation of eicosanoid biosynthesis is a routine function of GPx4 and that regulation of GPx4 expression may be part of the complex host-pathogen interaction. It was recently shown that Salmonella typhimurium modulates the

activity of the host antioxidant machinery by dampening GPx4 expression in intestinal epithelial cells (72). This occurs via a bacterial Type III secreted effector, SipA, and primes enterocytes to apically produce the pro-inflammatory 12-LOX product hepoxilin A_3, which governs the trans-epithelial migration of polymorphonuclear leucocytes associated with enteric infection. Suppression of GPx4 expression is discussed as a central mechanism governing the ability of S. typhimurium to evoke enteritis. Once again, whether this effect is shared with GPx1, the expression of which is also decreased by Salmonella, requires further investigation.

2 AIM

Due to the relevance of GPx4 in promoting cell survival, understanding the turnover of GPx4 is of pivotal importance. *In silico* analysis of GPx4 primary sequence indicated the presence of conserved LPXY motif at the C-terminal end. This motif is known for being recognized by proteins containing WW domains. Typically the substrates of the WW domains-containing E3 ligases of the Nedd4 family contain a C-terminal LPXY motif. Major aim of this work was therefore clarifying whether GPx4 could be a Nedd4 substrate, and thus proteasomal degradation could have a role in GPx4 turnover.

3 MATERIALS and METHODS

3.1 Cell cultures

Human embryonic kidney (HEK) 293T cell line was maintained in DMEM GlutaMaX containing inactivated FBS 10%, 100U/ml penicillin, 0.1 mg/ml streptomycin and 2 Mm L-glutamine (Life-Technologies). The medium was routinely supplemented with 100 nM sodium selenite (Sigma-Aldrich) in order to increase the expression of selenoproteins. All cells were incubated at 37°C in a humidified incubator containing 5% CO_2 and 95% air.

3.2 Reagents

Buthionine sulfoximine (BSO) (Sigma-Aldrich) was used in synergy with 500 uM Diethyl maleate (DEM) (Sigma Aldrich) to induce GSH depletion and sub sequently ferroptotic cell death. 1S,3R-RSL3 and 1R,3R-RSL3 , respectively active and inactive stereoisomers of RSL3 compound, are a kind gift from Institute of Clinical Molecular Biology and Tumor Genetics, Munich, Germany and used to obtain ferroptosis by direct GPx4 inhibition. α –tocopherol and Deferoxamine (Sigma-Aldrich) were used to verify whether, the induced cell death model, corresponds to ferroptosis. MG132 proteasome inhibitor (Sigma Aldrich) was utilized to block the proteasome system activity.

3.3 Constructs used for immunoprecipitation.

For the following experiments, the eukaryotic expression constructs pcDNA3.1HsV5-Nedd4.1^{wt}, pcDNA3.1HsV5-Nedd4.2^{wt}, pcDNA3.1HsV5-Nedd4.1$^{Cys/Ser}$, pcDNA3.1HsV5-Nedd4.2$^{Cys/Ser}$, (Cys-to-Ser mutation in the catalytic Cys of the HECT domain), and pcDNA3.1HsFLAG-YY1, alias Ying-Yang, well known substrate, ubiquitinated by Nedd4.1 and Nedd4.2, was a kind gift

from the Department of Biochemistry and Molecular Genetics of the University of Toronto (Canada).

3.4 Sequence alignment

ClustalW2 was the tool used for alignment of multiple amino acid sequences of GPx4 homologs.

3.5 Preparation of FLAG-tagged HsGPx4^{wt} and FLAG-tagged HsGPx4$^{LPHY/LAHA}$ expression vectors for eukaryotic cells.

Total RNA was extracted from human HEK293T cells by Trizol reagent (Life Technologies) and cDNA was obtained using 3ug of total RNA preparation and TaqMan® Reverse Transcription Reagents (Life Technologies). GPx4 cDNA was then cloned into the HindIII/XhoI restriction sites of pcDNA3.1 expression vector (Invitrogen) in the presence of a 5'-FLAG-tag using the following pair of primers, (see table1 below, pair 1) containing HindIII or XhoI restriction site (underlined) and FLAG tag (bolded). Primers were purchased from Sigma-Aldrich and Q5 Hot-Start High-Fidelity 2X Master Mix from BioLabs Inc. PCR cycles were then applied (98^{o} C for 1 minute, 98^{o} C for 30 seconds, 58^{o} C for 30 seconds, 72^{o} C for 30 seconds) for 38 cycles.

After PCR, the reaction was loaded into 1.5% agarose gel containing SYBER-Green for DNA purification and the DNA band visualized at 300 nm UV light. It was excised from the gel and purified by Wizard SV Gel and PCR Clean-Up System (Promega). The band and the pcDNA 3.1 vector were digested by HindIII/XhoI for 2 hours at 37 ^{o} C, purified by PCR Clean-Up System (Promega), eluted in water and ligated by T4 DNA ligase (Invitrogen) according to manufacturer's instructions.

Following PCR, was the reaction was loaded into agarose gel (Tris-acetate EDTA

buffer 1X, SYBER Green stock reagent 1:10 000, agarose 1%) for purification. Electrophoresis was performed at 120V and after visualizing the band at 300 nm UV light, the DNA band was excised from the gel for purification. DNA was purified by Wizard SV Gel and PCR Clean-Up System (Promega).

The Site-direct mutagenesis of LPHY motif of human GPx4 into LAHA was performed in two steps: first, the proline codon was mutated into alanine and then the tyrosine codon was converted into alanine using the primers indicated in the table1 by QuickChange site-directed mutagenesis kit (Agilent).

name	Forward 5'-3'	Reverse 5'-3'
GPx4 cloning and FLAG insertion	ATAAAAGCTTGCCACCATG**GACTAC AAAGACGATGACGACAAG**TGCGCG TCCCGGG	ATTACTCGAGGCAGGCTAATTTGTC TGTTTATTCCCACAA
Pro (CCC) into Ala(GCC)	GGTGATAGAGAAGGACCTGGCCCAC TATTTCTAGCTCCAC	GTGGAGCTAGAAATAGTGGGCCAG GTCCTTCTCTATCACC
Tyr (TAT) into Ala (GCT)	GATAGAGAAGGACCTGGCCCACGCT TTCTAGCTCCACAAGTG	CACTTGTGGAGCTAGAAAGCGTGG GCCAGGTCCTTCTCTATC

Table 1. Primers for GPx4 cloning in pcDNA3.1 and insertion of 5' FLAG-tag. Primers for site-direct mutagenesis of Pro and Tyr into Ala in LPHY motif of GPx4

3.6 E. coli transformation and isolation of plasmid DNA

DH5α E.coli strain was used for transformation to obtain sufficient amount of the cloned construct. 3 µl of the above ligation reaction was added into a tube containing 50 µl of DH5α. The mixture was incubated on ice for 20 minutes, followed by heat shock at 42^{o} C for one minute and incubated on ice for 2 minutes. 600 µl of Luria-Bertani broth (# L3022 Sigma-Aldrich) was added into

the tube and then incubated for 30 minutes on 37^{o} C with shaking (222 rmp). Cells were plated on LB-agar containing ampicillin and incubated over night at 37^{o} C. Grown bacterial colony from LB plate was picked and incubated in 8/10 ml LB containing ampicillin overnight at 37^{o} C with shaking for further isolation of plasmid DNA.

3.7 Immunoprecipitation of FLAG-tagged GPx4 and in vivo ubiquitylation assay

The method was performed according to Persaud, A. et al, Molecular Systems Biology (2009) (73).

HEK293T were co-transfected (using Gene Jammer reagent, Agilent) with FLAG-tagged substrates (YY1, positive control or HsGPx4^{wt} / HsGPx4$^{LPHY/LAHA}$ substrates of interest) and either V5-tagged hNedd4.1^{wt}, V5-tagged hNedd4.2^{wt} , V5-tagged hNedd4.1$^{Cys/Ser}$ or V5-tagged hNedd4.2$^{Cys/Ser}$ (Cys-to-Ser mutation in the catalytic Cys of the HECT domain) for a total amount of 15.8 µg DNA per T75cm^{3} . For the binding and ubiquitylation assays, cells were treated with 20 µM proteosomal inhibitor MG132 (Sigma Aldrich) for 3 hours before the lysis (50mM Tris-HCl pH 7.4, 150mM NaCl, 1% Triton X-100, 10% glycerol, 1.5mM MgCl2, 1.0mM EDTA, 10 mg/ml leupeptin, 10 mg/ml aprotinin and 1mM PMSF) supplemented with 50 mM LLnL (N-acetyl-Leu-Leu-norleucinal; Sigma) and 0.4mMchloroquine (Sigma). Samples were centrifugated at 17 000 x g for 15 min.

Only for ubiquitylation assa, to ensure specific ubiquitylation of the FLAG-tagged substrate, and not of associated proteins, 600-800 µg of cleared cell lysate was treated with 1% SDS and boiled at 95°C for 5 min, as a 'pre-cleaning' procedure. The lysates, previously subjected or not pre-cleaning step, were then diluted 11 times with lysis buffer (to dilute detergents) before immunoprecipitation, for incompatibility with the FLAG-matrix. Lysates were then incubated with 30 µl of Anti- Flag M2 affinity agarose (Sigma) at 4°C for overnight. Bound proteins were washed trice with wash solution (0.1M Tris-HCl pH 7.4, 0.3M NaCl, EDTA 1mM,

10% glycerol, CHAPS 0.1%). Co-immunoprecipitation of NEDD4 proteins were detected by immunoblotting with anti-V5 antibody. Ubiquitylation was detected by immunoblotting with anti-ubiquitin (Ub)

The antibodies used for immunoblotting were: anti-ubiquitin antibody (1:300 dilution; Cayman), anti-Flag antibody (1:1000 dilution, Sigma Aldrich), anti-V5 antibody (1:2000 dilution; Sigma Aldrich). The secondary antibody was incubated for 30 minutes (1:2000 dilution; goat-anti mouse HRP-conjugated; Santa Cruz) and further developed on Kodak image station using Luminol solution.

3.8 Production of GST-tagged Nedd4.1

pGEX-5X-3-GST-Nedd4.1.WT was a kind gift from Toshiaki Fukushima of the Department of Animal Sciences and Applied Biological Chemistry of the University of Tokyo. *E.coli* bacteria BL21(DE3 PLysS) were transformed with the recombinant vector. A single transformed colony was grown in 50 ml of Luria Bertani Medium (LB medium) (Sigma-Aldrich) containing 100 µg/ml ampicillin at 37°C with shaking at 220 rpm. After overnight growth, 20ml of the bacterial culture was added to 2 liters of LB medium containing ampicillin for exponential growth. When the OD_{600} value monitored spectrophotometrically reached 0.6, the growth was inducted with 1 mM isopropyl-β-D-thiogalactopyranoside (IPTG) (Thermo Fischer). The culture was then incubated for another 4 hours at 37°C with shaking at 220 rpm. The bacterial culture was centrifuged at 5000xg at 4°C for 30 minutes. The obtained pellet was ready to resuspended in Bacterial Protein Extraction Reagent (BPER) (Cell BIO) containing pepsatin 0.7 mg/ml and leupeptin 0.5 mg/ml, and left for 10 minutes in slow agitation at 4°C. The cell lysate was dissolved by sonication, and centrifuged (35 000 x g, 30 minutes, 4°C).

3.9 Purification of GST-tagged Nedd4.1

A pellet obtained from 1 liter of bacterial culture was extracted using 100 ml of B-PER™ buffer (Nonidet 5%, 20 mM Tris-HCl pH 7.4, Pepsantin 0.7 mg/ml, Leupeptin 0.5 mg/ml-mix bacterial protease inhibitor, Sigma Aldrich). The resuspension of pellet was performed at 4°C for 20 minutes in slow agitation. The crude extract, was centrifugation at 35.000xg for 30 minutes at 4°C (BECKMAN OPTIMA L-9K0) and diluted 1:3 using the column equilibration buffer (PBS) pH7.0. Next, sample was applied to 1 mL HITrap FF column, connected to ACTA PURE apparatus (GE healthcare) at flow rate of 0.2 ml/min. To bind the GST-tagged Nedd4.1, washing was performed for 30 minutes by PBS at flow rate of 1mL/min and at the end, elution of the protein was performed by elution buffer (50 mM Tris-HCl, 10 mM Glutathione pH 8.0) at flow rate of 1mL/min. The fractions were collected in volume of 1ml and the presence of recombinant protein was identified by SDS-PAGE 12% and staining with Comassie Brillant Blue (CBB). The enriched fractions were pooled together, quantified using Bradford reagent (Sigma-Aldrich) and stored at -80°C.

3.10 In vitro ubiquitylation assay

Purified GPx4 was obtained from rat testis as described by Roveri A. et al. (1994, Biochim Biophys Acta) (74)

3.6 µg of purified rat GPx4 was mixed with 150 ng His tagged-human ubiquitin activating enzyme E1 (Enzo Life Sciences), 300 ng His-human UbcH5b (Enzo Life Sciences), 750 ng recombinant GST-Nedd4.1. produced as described above, 7.5 mg ubiquitin (Sigma-Aldrich) and 2 mM ATP, in the reaction buffer (25 mM Tris-HCl pH7.5, 120 mM NaCl, 0.5 mM dithiothreitol and 2 mM MgCl2). After the incubation at 30°C for 2 hours, samples were washed four times, followed by SDS-PAGE 12% and immunoblotting with anti-ubiquitin antibody.

3.11 Preparation of the cytosol

At the end of the experimental times, cells were collected from T75 cm^3 flask and resuspended in 300uL of homogenization buffer containing 10mM Tris-HCl, pH 7.4, 1mM EDTA, 0.25M Sucrose, 1% protease inhibitor (protease inhibitor cocktail, Sigma). A mechanical lysis was performed to facilitate the rupture of the external membranes by glass-glass potter (100 strokes). Obtained lysate was then centrifuged at 300xg, 4°C for 10 minutes to discard intact cells. The obtained supernatant was ultra-centrifuged at 105.000xg, 4°C for 1h to obtain the cytosolic fraction As the supernatant of the centrifugation, for western blotting analysis residual pellet was suspended in Laemmly buffer in the same volume of cytosolic fraction.

3.12 Protein measurement by the Lowry assay.

Protein content was measured according to Lowry as modified by Bensadoun et al., (1976, Anal. Biochemistry) (75) taking advantage of previous DOC-TCA precipitation. Samples were first diluted to 3 mL final volume with water, containing DOC. A minimal volume of diluted DOC detergent was then added to a final concentration of 0.02% (w/v) followed by 1 mL of diluted TCA to a final concentration of 6 %. Sample was left to incubate 10' on ice, before spinning it down at 3800xg for 30 minutes at 4°C. Supernatant containing soluble contaminants was then discarded carefully. A solution of 2% Na2CO3 (w/v), 0.1 N NaOH and a solution of 0.5% CuSO4 (w/v), 1% KNaTartrate (w/v) were mixed together to a ratio of 50:1 prior to use and each precipitated sample pellet was dissolved into 1 mL of the resulting solution and incubate at room temperature in the dark. After 30 minutes 0.1 mL of freshly 1:1 water diluted Folin's reagent (SIGMA) was added to each sample and samples were incubated for additional 30 minutes at room temperature in the dark. At the end of incubation period, sample absorbance was recorded at 750 nm with Cary 50 UV-Vis spectrophotometer (Agilent Technologies). Sample concentration was then

calculated by referring to a standard curve ranging from 1 to 10 ug of bovine serum albumin (BSA) prepared in the same buffer of protein samples to be measured.

3.13 Total GSH measurement by the Tietze assay

Tietze assay is the method first described in 1969 to measure the glutathione content (76). It is based on the principle that GSH can be measured by an enzymatic recycling procedure in which it is sequentially oxidized by 5-5'-dithiobis [2-nitrobenzoic acid] (DTNB, Ellman's Reagent), forming the 412 nm cromophore 5-thionitrobenzoic acid (TNB) and GS-TNB. Any GSSG in the sample is reduced by NADPH and glutathione reductase (GR) to GSH, thus the total GSH in the sample is measured. Reduction of GS-TNB by NADPH and GR releases a second TMB molecule and recycles the GSH, thus amplifying the response. The rate of formation of TNB, which is proportional to the total glutathione amount, can be followed using a spectrophotometer. Total glutathione is quantitated by referring to a standard curve.

The amount GSH was then calculated with reference to a standard curve ranging from 0,001 to 0,01 mg/mL (from 16-160nmolies) of oxidized or reduced glutathione in water.

Pratically, each sample of a volume of 5-10uL were diluted in buffer, containing 0.1M Na-phosphate, pH7.3, 1mM EDTA, 10mM DTNB, NADPH and the reaction started by adding 0.004units/mL of Glutathione reductase (Sigma Aldrich).

Total glutathione was measured as rate of TNB formation at 412nm.

3.14 GPx4 activity assay in cell lysate

HEK293T were lysed as reported above by lysis buffer (10mM Tris-HCl, pH 7.4, 1mM EDTA , 0.25M Sucrose, 1% protease inhibitor) and lysis buffer was exchanged using NAP-5 column (GE Healthcare). The column was equilibrated

with the buffer for measuring and containing 0.1 M Tris-HCl pH 7.8, 5 mM EDTA, 0.1% Triton X-100 and 3 mM GSH. The same buffer was used to eluted the samples. GPx4 enzymatic activity measurement was determined by a coupled spectrophotometric assay, performed at 340 nm where GSH consumption in the presence of enzyme specific substrate, phosphatidylcholine hydroperoxide (PCOOH), is coupled to NADPH consumption by glutathione reductase. The measurement was carried-out using Cary 50 UV-Vis spectrophotometer (Agilent Technologies). After baseline recording, the reaction, containing 100 µg of total protein concentration, was started by adding 30 µM of a specific GPx4 substrate - PCOOH in the activity buffer where 0.16 mM NADPH and 2 U/ml glutathione reductase were added. GPx4 activity was calculated using NADPH extinction coefficient E_{NADPH}= 6.22 mM^{-1} cm^{-1}. PCOOH was prepared according to Maiorino et al. (1990, Metod. Enzymol.) (20)

3.15 SDS-PAGE and western blotting analysis

50ug of the sample (e.g. cytosol or membrane preparation) was diluted in Laemmli buffer (62.5mM TrisHCl pH 6.8, 2.5% SDS, 10% glycerol, 1 M β-mercaptoethanol, 0.004% pironine), denaturated by heating to 95°C for 5 minutes and loaded into home-made to 15% polyacrylamide gel. SDS-PAGE Molecular Weight Standars (BioRad) were used as molecular weight marker. Separation was performed using running buffer prepared freshly each time, at three different steps: 5mA, 10 mA and 20 mA, each step during for 1h. The electrophoresed samples were trans-blotted onto nitrocellulose membrane at 180 mA constant current overnight using blotting buffer (25mM ethanolamine, 0.10 M glycine and 20% v/v methanol pH 9.5). The success of transfer was verified by Ponceau red staining (0.2% (w/v) in 3% (v/v) TCA aqueous solution. The nitrocellulose membrane containing transferred proteins was saturated by Tris buffered saline (TBS) containing 0.1% Tween-20 and 3 % BSA for two hours and incubated overnight with home-made rabbit affinity purified anti-GPx4

antibody (1:250) following the incubation with anti-rabbit secondary antibodies (1:4000) (Santa Cruz). The same membranes were incubated with primary antibody against B-actin (1:2000) (Santa Cruz) and relative anti-mouse secondary antibody to normalize the results. In some experiments anti-Ub antiboby (1:300) (caymann) was used. The membrane was washed three times with TBS Tween 0.1% and developed with luminol chemiluminescent reactions at Kodak Image Station using luminol solution (1.1 mM luminol, 1 mM 4-iodophenol, 0.12% BSA, 1.4 M H_2O_2, 0.025 mM Tris-HCl pH 9.25).

3.16 Cell viability measurement

Cell viability was measured with Alamar Blue/Resazurin (Sigma Aldrich). Cells were seeded at a density 12.000cells/well in 96 wells plates with the complete growth medium. After 24h, the growth medium was discarded and the cells were starved with serum-free medium. The following day, the cells were treated with GSH depleting agents 5mM BSO and 500 µM DEM in medium without serum, with or without 400 µM α-tocopherol or 400 µM-Deferoxamine (Sigma-Aldrich). At the selected experimental time, this was then replaced with fresh growth medium that, the day after, was supplemented with 100uM Alamar Blue. Fluorescence was measured by FluoScan (ThermoSystem, ex. 544 nm ±15, em. 590±14). Resazurin reduction rate was evaluated as A.F.U/min, and expressed as % vs. control.

3.17 Lipid peroxidation measurement

Lipid peroxidation was detected by BODIPY 581/591 C11 staining (Thermo Fischer). Cells were seeded at a density of 200.000 cells/well in 6 wells plates. After 24h, the growth medium was discarded and the cells were starved with serum-free medium. The following day, the cells were treated with GSH depleting agents for selected experimental time, as above. An hour before of

harvesting, 1 uM BODIPY 581/591 C11 (staining) was added. After 2hours, cells were harvested, washed in PBS and resuspended in 300 uL PSB for flow cytometry analysis (BD, FACS, CantoII, equipped with a 488nm excitation laser). Fluorescence of C11-BODIPY was measured by simultaneous acquisition of the green (535 nm) and red signal (585 nm). 6 wells plates without BODIPY were monitored to allow the subtraction of self-fluorescence. The results are expressed as ratio (535nm/585nm) after subtraction of the individual blank.

3.18 Surface Plasmon Resonance (SPR) analysis

Reagents

Phospholipids: 1,2-Dioleoyl-sn-glycero 3 phosphocoline (DOPC), 1,1'2,2'-Tetraoleoyl Cardiolipin (TOCL) were all from Avanti Polar Lipids, USA. 3-Phosphatidic acid, Octyl Glucosyde (OG), isopropanol, Hepes, Tris, GSH, bovine serum albumin (BSA) and bovine GPX1 were purchased from Sigma. GPX4 was purified from rat testis, as described by Roveri A. et al. (1994, Biochim Biophys Acta) (74). All solutions were freshly prepared and filtered through a 0.22 µm filter.

Liposome preparation

Phospholipids were dissolved in chloroform/methanol/water (65:35:8) and different lipids mixtures were prepared by mixing separately TOCL in the desired ratio with DSPC in a glass tube. After chloroform and methanol have been removed by nitrogen flux, the dried phospholipids mixtures were resuspended in 2 mL of buffer (10 mM HEPES, 150mM NaCl, pH 7.4, final lipids concentration 1mM) and vigorously stirred by vortex for 2 minutes. Liposomes were finally obtained by extruding 10 times the lipids suspensions through 0.1 µm polycarbonate filters (Whatman Nuclepore Track Etched Membranes), at 50°C, using an extruder (Lipex Liposome extrusion system).

Lipid Immobilization on the SPR sensor chips

Surface Plasmon Resonance (SPR) experiments were carried out at 25°C with a Biacore T100 analytical system (Biacore, Uppsala, Sweden), using an L1 sensor chip (Biacore). All four sensor chip channels were used, immobilizing a different lipid mixture on each. Before immobilizing the lipid bilayers, the lipophilic sensor chip surface was cleaned by 40 mM octyl glucoside and isopropanol/50mM NaOH (2:3). The deposition of the lipid bilayers onto L1 surface was carried out injecting the liposome suspensions for 25min with 4 µL/min flow rate. To this purpose, 10 mM HEPES, 150mM NaCl, pH 7.4 was used as running buffer. After the liposome injection, 10 mM NaOH was introduced for 60 s at 10 µL/min to remove the loosely bound liposomes. 0.1mg/mL of BSA was then injected for 300 s at 10 µL/min to seal the gap in the phospholipid layer to avoid non-specific binding. After the BSA injection a solution of 10 mM NaOH and then a solution of 2M KCl were introduced at 10 µL/min for the baseline stabilization.

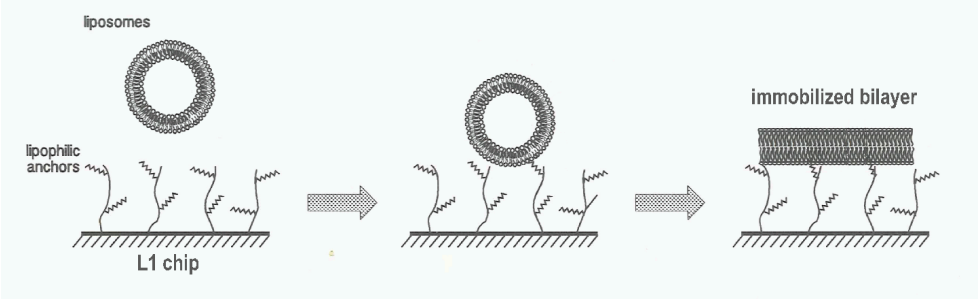

G. Stepanov, O. Gnedenco, A. Mon'lar, A. Ivanov, Y. Vladimirov, A. Os ipov.

valuation of cytochrome c affinity to anionic phospholipids by means of surface plasmon resonance. *FEBS Letters 583* (2009) 97-100.

R. Järving. A. Lõokene, R. Kurg, L. Siimon, I. Järving, N. Samel.

SPR analysis of GPx4 binding to extruded liposomes

Rat testis GPx4 purified as described (74), was injected onto the immobilized phospholipid bilayers for 180s passing through all the four sensor channels at a flow rate of 30 µL/min. Than the running buffer (composed as indicated below) was let to flow for the protein dissociation. After a dissociation period of 300-600s, 2M KCl and 50mM NaOH was injected for 30s to remove the still bound GPx4 and regenerate the phospholipid bilayer surfaces. GPx4 concentrations used were in the range of 0.05-5µM, while 25mM Tris, at pH 7.4, with or without 150mM KCl was used as running buffer for all the experiments. When 5mM GSH was introduced into the buffe, pH was corrected with KOH at 7.4.

Biacore T100 Evaluation Software 2.0.3 (GE) was used for data analysis, and the apparent K_D constant was calculated by fitting the experimental data to the equation:

$$R_{eq} = R_{max} \cdot C/(K_D+C) \qquad (1.3)$$

where R_{eq} represents the equilibrium binding level, C is the GPx4 concentration and R_{max} is the maximum value of the biosensor signal.

3.19 In silico studies

GPx4 structure was retrieved from Protein Data Bank (PDB code: 1OBI) and processed in order to remove unwanted ligands and water molecules. Hydrogen atoms were added to the protein structures using standard geometries. To minimize contacts between hydrogens, the structures were subjected to Amber99 force-field minimization until the rms (root mean square) of conjugate gradient was < 0.1 kcal $\cdot$ mol^{-1} $\cdot$Å^{-1} (1 Å = 0.1 nm) keeping the heavy atoms fixed at their crystallographic positions.

Molecular Dynamics simulation of GPx4-membrane system.

Molecular dynamics (MD) simulation of GPx4-membrane complex was performed with NAMD and ACEMD for 400 ns (NPAT, 1atm, 300 K, AMBER force-field) after an equilibration phase of 10 ns (positional restraints were applied on carbon atoms to equilibrate the solvent). Membrane system containing 50% PC and 50% CL (200 phospholipid molecules total), water molecules and ions atoms, was previously build and equilibrated. Hydroperoxide was parameterized and introduced at position 9 and 13 of TLCL (CL containing four linoleic acid chains). After 50ns the hydroperoxide group (TLCL, 9/13-OOH) moves up becoming close to lipid water interface, and solvent exposed after 130 ns. TLCL-OOH pose from MD simulation was used for a molecular docking procedure against GPx4 using a Genetic Algorithm; the complex GPx4-TLCL, was then submitted to the MD simulation process in membrane system.

4 RESULTS

Sequence analysis of vertebrate GPx homologs reveals that GPx4 peculiarly contains a conserved LPXY motif at the C terminus (Fig. 11). This motif is known to bind the so-called WW domains in proteins. WW domains are a small peptide binding domains of approx. 38 aminoacids, which are contained, among others, in the E3 ligase Nedd4 family members (Fig. 12). We therefore investigated whether GPx4 is a Nedd4 substrate and if Nedd4 is involved in GPx4 destabilization following protein inactivation.

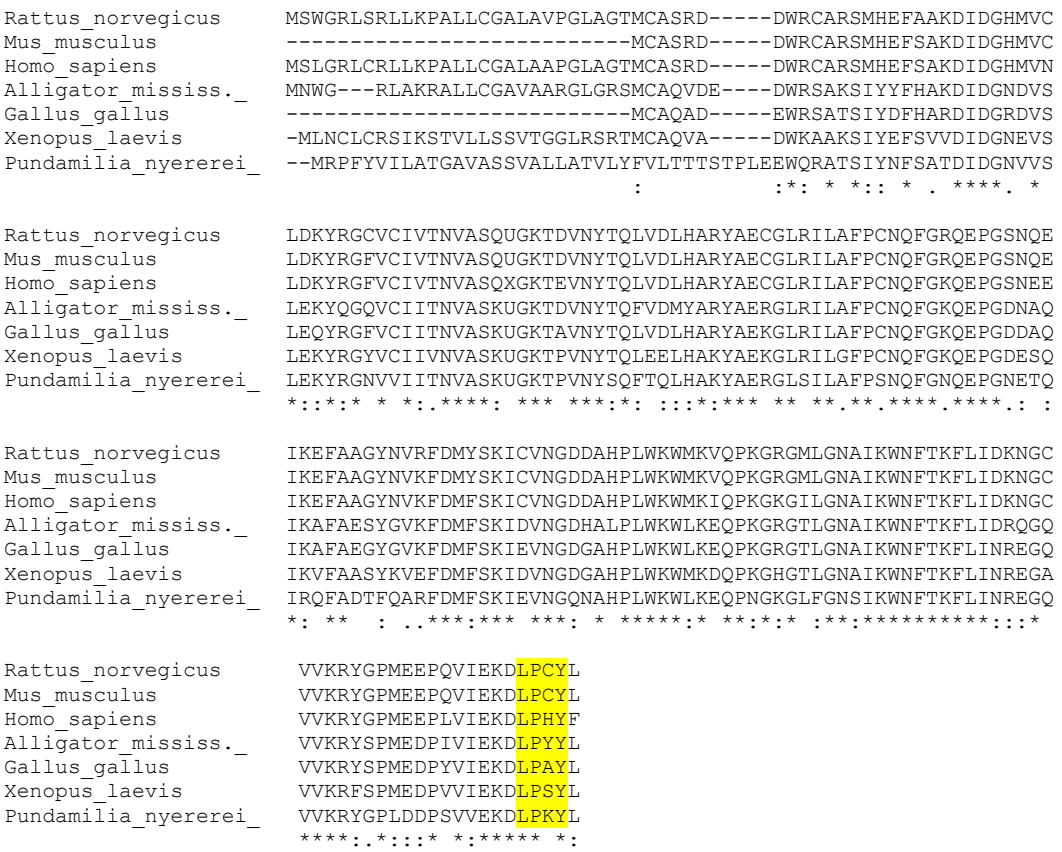

Figure 11. Primary sequence alignment of GPx4 from different vertebrates (*Rattus norvergicus, Mus musculus, Homo sapiens, Alligator mississippi, Gallus gallus, Xenopus laevis, Pundamilia nyererei)*. Note the conserved LPXY motif at the C-terminus

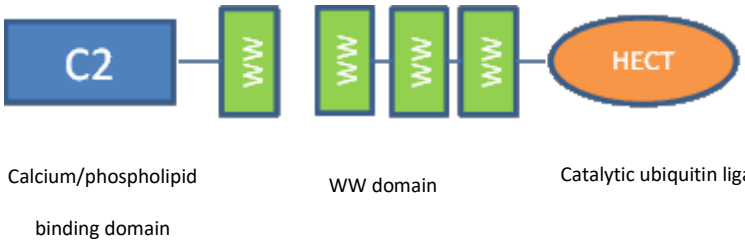

Figure 12. Structural organization of the HECT ubiquitin (UQ) ligases of the Nedd4 family. Nedd4 contains a variable (2-4) number of WW domains, a C2 domain and ubiquitin ligase HECT domain that are involved in the binding and ubiquitylation of protein substrates containing the LPXY motif (77)

4.1 GPx4 binds to Nedd4 and the LPHY motif of the peroxidase is relevant to the binding, but, apparently, GPx4 is not ubiquitylated by Nedd4.1

4.1.1 *In vivo* binding analysis

The two major isoforms of Nedd4, Nedd4.1 and Nedd4.2, sharing each other 67% identity, were tested in an *in vivo* binding analysis for their ability to interact with GPx4. To this end, HEK293T cells were co-transfected by a eukaryotic vector expressing FLAG-tagged human GPx4 wild type (pcDNA3.1FLAG-HsGPx4^{wt}) and a eukaryotic vector expressing V5-tagged human Nedd4.1 wild type or human Nedd4.2 wild type (pcDNA3.1V5-HsNedd4.1^{wt} or pcDNA3.1V5-HsNedd4.2^{wt} respectively). After cell lysis and immunoprecipitation by the FLAG matrix, western blot (WB) analysis using anti-V5 antibodies was performed. Results in Figure 13 show that, invariably, Nedd4 is present in the immunoprecipitate obtained by the FLAG matrix, indicating that GPx4 binds to both, Nedd4.1 and Nedd4.2 (Fig. 13A).

To highlight the role of the GPx4 C-terminal LPHY motif in this interaction, we set up a similar experiment where a FLAG-tagged vector carried a LAHA motif replacing the LPHY motif of human GPx4 (pcDNA3.1FLAG-HsGPx4$^{LPHY/LAHA}$) was

used as substrate for the two Nedd4 isoforms. The signal obtained following FLAG immunoprecipitation and WB analysis was compared to that obtained with cells co-transfected by pcDNA3.1FLAG-HsGPx4^{wt}. Results in Fig. 13B show a clear decrease of the intensity of the anti-V5 signal when the mutated construct was used as substrate for Nedd4.1 or Nedd4.2, thus indicating that the LPHY motif is involved, at least in part, in the interaction between Nedd4.1 or Nedd4.2 and GPx4.

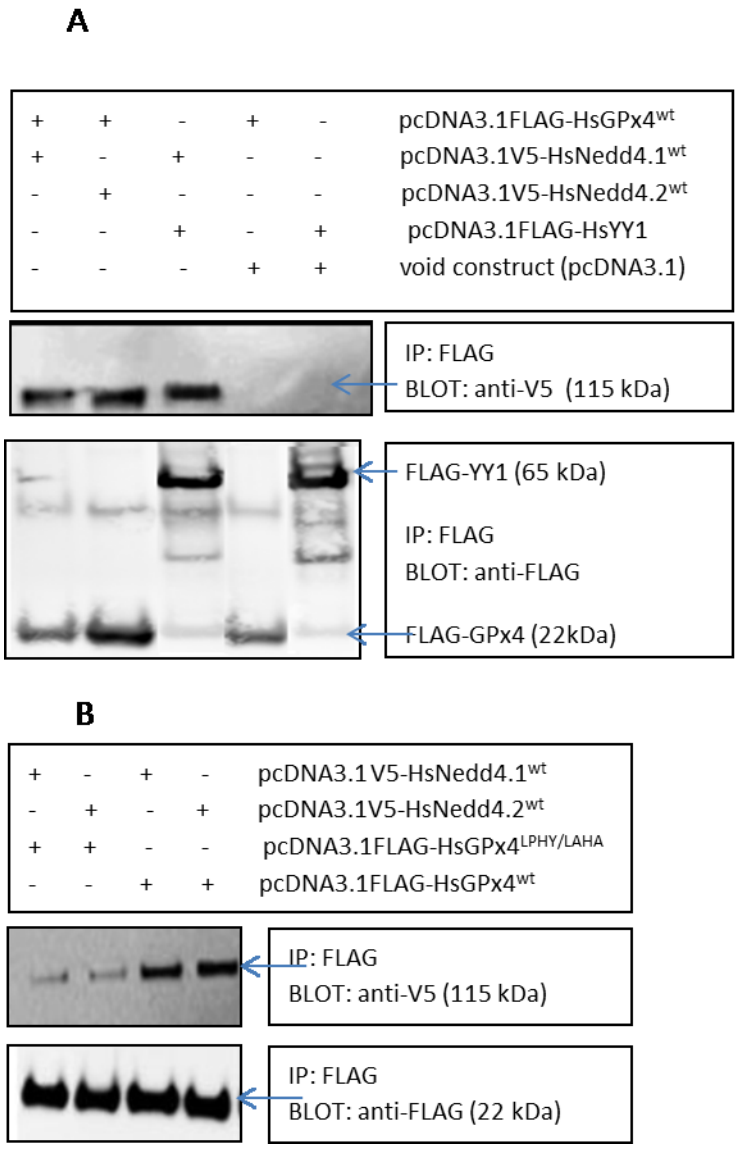

Figure 13. Interaction between GPx4 and Nedd4 isoforms in vivo binding analysis (A) and role of the C-terminal LPXY motif in GPx4 (B). HEK293T cells were used (A) After co-transfection with the indicated constructs, cells were lysed and immunoprecipitated by the FLAG matrix. The obtained immunoprecipitate, containing therefore FLAG-tagged GPx4, was analyzed by western blot and

decorated (top) by the V5 antibody to detect V5 tagged Nedd4 isoforms or bottomteh anti-FLAG antibody to detect GPx4 or YY1. pcDNA3.1FLAG-HsYY1 is the expression construct encoding for the positive control (the transcription factor Yang-Yang1). pcDNA3.1 is the empty vector used as control (see methods for detail). In (B) the experiment was performed as above except that, in some experiments, a vector carrying a LAHA motif replacing the LPHY motif of human GPx4 (pcDNA3.1FLAG-HsGPx4$^{LPHY/LAHA}$ was used as substrate for Nedd4.1^{WT} or Nedd4.2^{WT}, as indicated.

4.1.2 *In vivo* ubiquitylation analysis.

We next addressed whether the binding between the Nedd4 isoforms and GPx4 targets the peroxidase for ubiquitylation, by an *in vivo* ubiquitylation analysis.
Since in the HECT ubiquitin (Ub) ligases homologs, differently from other ligases involved in ubiquitylation (e.g the RING homologs), an obligate high energy thioester bond is formed between the catalytic Cys residue of the ligase and the C-terminal carboxylate of Ub, an expression constructs carrying a mutated form of the catalytic Cys of the two Nedd4 isoforms was built. The aim was to highlight the specific involvement of these ligase isoforms in the ubiquitylation of GPx4. The mutated construct carried the active site Cys in the HECT domain of Nedd4.1, or Nedd4.2, mutated into Ser (pcDNA3.1V5-HsNedd4.1$^{Cys/Ser}$ or pcDNA3.1V5-HsNedd4.2$^{Cys/Ser}$). These, or the Nedd4.1^{wt} or Nedd4.2^{wt} expression constructs were co-transfected together with pcDNA3.1FLAG-GPx4^{wt}. To prevent ubiquitylated protein degradation by the proteasome, co-transfected cells were also treated for 3h with 20 µM MG 132, a well-known proteasome inhibitor. Notably, in these experiments, following immunoprecipitation of the lysates by the FLAG matrix a 'pre-cleaning procedure' was made, which was aimed to remove any unspecific ubiquitylated protein associated to the immunoprecipitate. This 'pre-cleaning procedure' consisted in boiling for 5 min the immunoprecipitate after 1% SDS was added. After centrifugation, the pellet was washed and analyzed by WB using anti-Ub antibodies. Results are presented in Fig. 14: the FLAG immunoprecipitate containing GPx4 reacted indeed with the Ub antibodies either in the cells transfected with Nedd4.1^{wt} or Nedd4.2^{wt} (Fig. 14A), and a smear of reactivity was observed, indicating polyubiquitylation.

Unfortunately, however a similar signal was also present in cells transfected by the mutated constructs (i.e. pcDNA3.1V5-HsNedd4.1$^{Cys/Ser}$ pcDNA3.1V5-HsNedd4.2$^{Cys/Ser}$, Fig. 14B).

The possibility that proteins other than GPx4 contributed to the Ub signal in the FLAG immunoprecipitate, was tentatively addressed by increasing the SDS concentration in the 'precleaning procedure'. Indeed, by increasing the concentration of SDS to 1.5% we obtained a lack of Ub signal in the experiment where GPx4 was used as a Nedd4.1 substrate, but, unfortunately, a lack of Ub signal was also observed in the lane containing the positive control, where pcDNA3.1FLAG-HsYY1 was used as Nedd4 substrate (not shown).

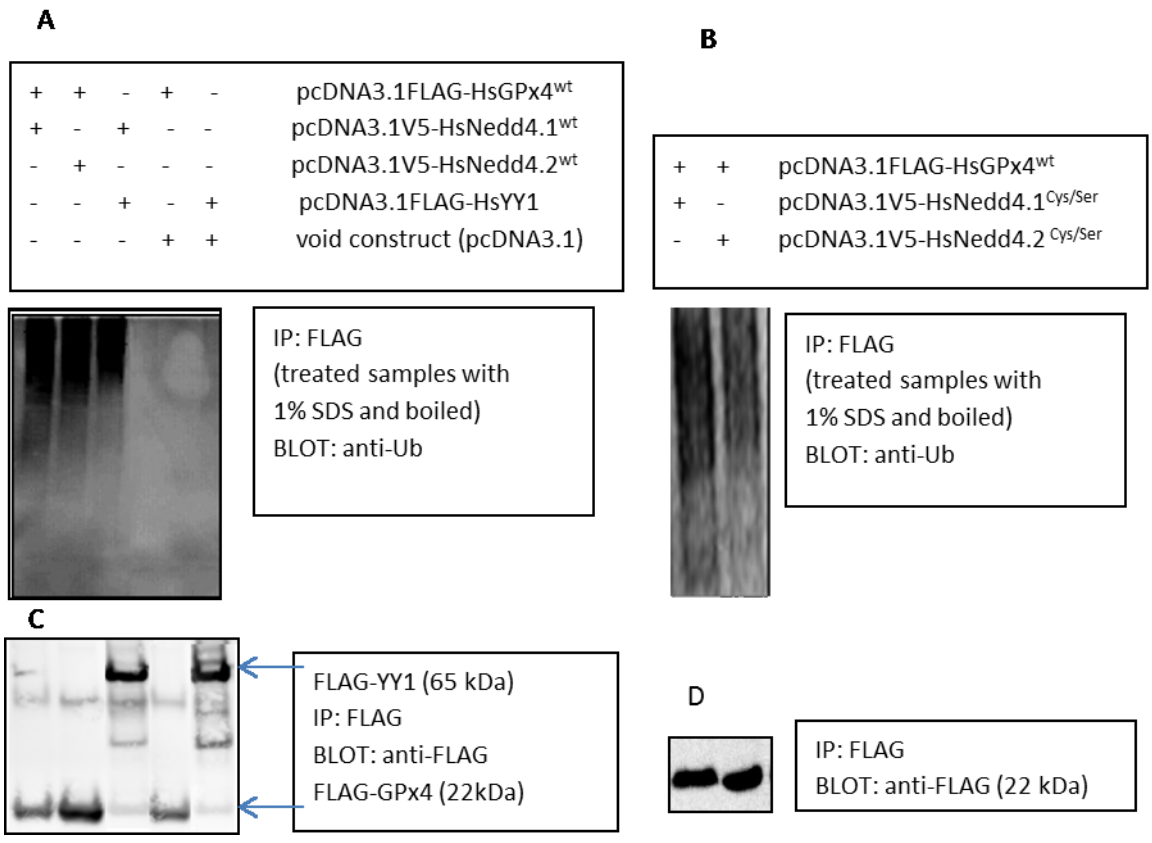

Figure 14. *In vivo* ubiquitylation analysis of human GPx4 in the presence of human Nedd4 isoforms. HEK293T cells were used and co-transfected with the constructs indicated in the figure. Wild type (A) or Cys-to Ser mutated Nedd4 isoforms (B) were used as E3 ligase source. After cell lysis, immunoprecipitation by the FLAG matrix and pre-cleaning of the immunoprecipitate, the pellet was analyzed by WB and decorated with the anti-Ub antibody.

Note that the sample that was co-transfected with catalytic Cys mutated Nedd4 isoforms, (B), yields a Ub signal similar to the those containing the WT Nedd4 isoforms, (A). (C) and (D): in presence of GPx4 or YY1 was demonstrated with FLAG immunoprecipitate obtained from the experiment in panel (A) and (B) respectively.

4.1.3 *In vitro* ubiquitylation assay

Since previous experiments failed to give a clear-cut answer to the question whether GPx4, besides binding to, is ubiquitylated by Nedd4 isoforms, we set up an *in vitro* ubiquitylation assay (Fig. 15), where the entire system for ubiquitylation (e.g. E1, E2, E3, ATP, Ub and GPx4) is present in a purified form and reacts together in an appropriate buffer (Fig. 15). To this end the Nedd4.1 E3 ligase was obtained by cloning, expressing and purified GST-tagged HsNedd 4.1, while GPx4, the hypothetic E3 substrate, was purified by rat testis. E1, E2 and Ub were commercially available proteins. The reaction mixture, following 2h incubation at 30°C was analyzed by WB and decorated by anti Ub antibody (Fig. 15). Unfortunately, results did not provided evidence for GPx4 ubiquitylation by purified Nedd4.1, at least under the adopted conditions. Indeed an identical smear of ubiquitylated proteins was observed in the presence and in the absence of GPx4 (Fig. 15A). However, the fact of the system was working properly, is demonstrated by the observation that ubiquitylation did not occur if ATP was omitted from the mixture (Fig. 15B) or if the incubation system did not contain all the required components (Fig. 15A). All together these experiments unequivocally indicate that our purified Nedd4.1 is catalytically active, and that the E1 or the E2 enzyme or Nedd4 enzymes itself, but not GPx4, undergo ubiquitylation by Nedd4.1. This view is as well confirmed by the observation that, following the reaction, GPx4 is revealed at the expected MW by anti-GPx4 antibody (Fig. 15C)

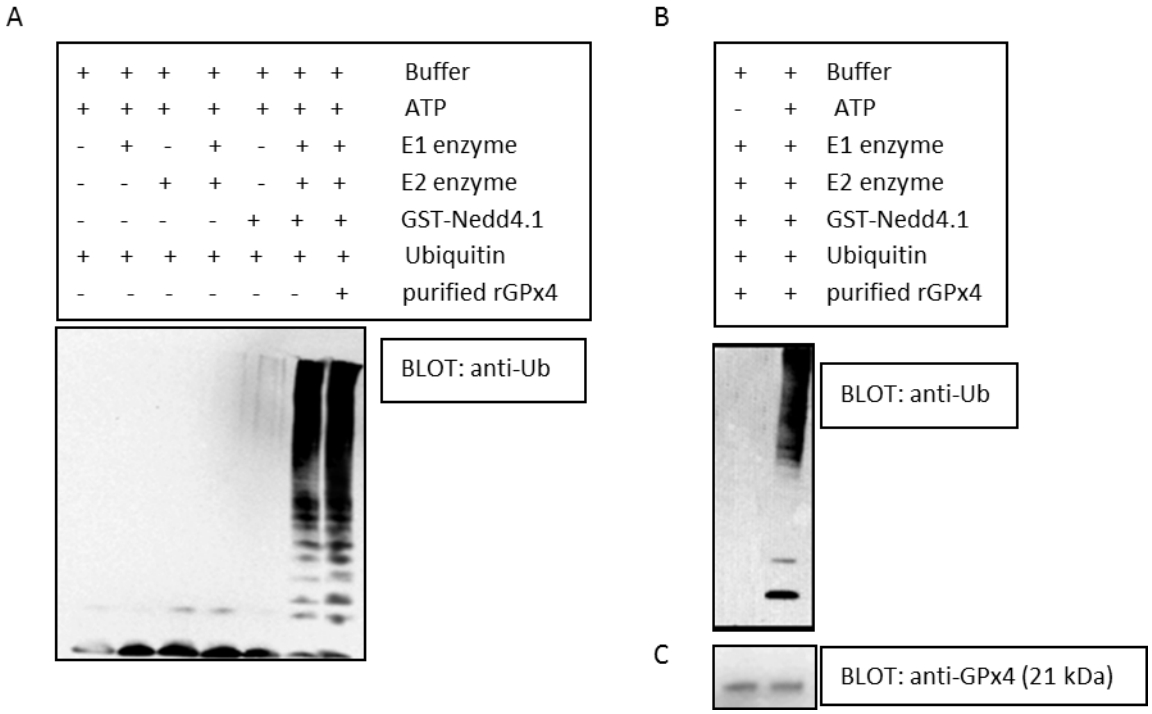

Figura 15. *In vitro* ubiquitylation of GPx4 by purified Nedd4.1. (A) Top: the components present in each sample are indicated, Bottom: corresponding WB analysis decorated by anti-Ub antibody. Note that the lane where GPx4 is omitted show the same ubiquitylation pattern as the lane where GPx4 is present; (B) Effect of ATP on the ubiquitylation reaction; (C) The blot was stripped and decorated by GPx4 antibody. Note that there is not evidence of poly- or mono-ubiquitylation, since the proteins is detected without any smear at the expected MW.

We reasoned that an incorrect conformation of the peroxidase could be the reason underlying the negative results so far obtained by the *in vitro* ubiquitynation assay. We decided therefore to address whether Nedd4.1 has any role in the clearing of GPx4 *in vivo* in HEK293T cells. A series of experiments were planned, where the amount of endogenous GPx4 in cells, measured as specific activity and/or as a protein in WB), was compared as a function of time in cells overexpressing or not the Nedd4.1 isoform.

4.2 Nedd4.1 overexpression does not modify GPx4 turnover in normal cells

First, we addressed whether overexpression of Nedd4.1 could affect GPx4 turnover in non-challenged (i.e. normal) cells. To this end HEK293T cells were transfected with Nedd4.1 expression construct or with an empty construct and the amount of endogenous GPx4 by western blotting was measured in a time frame of 24 hours. Results in Fig. 16 show that overexpression of Nedd4.1 did not affect the clearance of GPx4, indicating that the turnover of GPx4 is not influenced by Nedd4.1 in unchallenged cells.

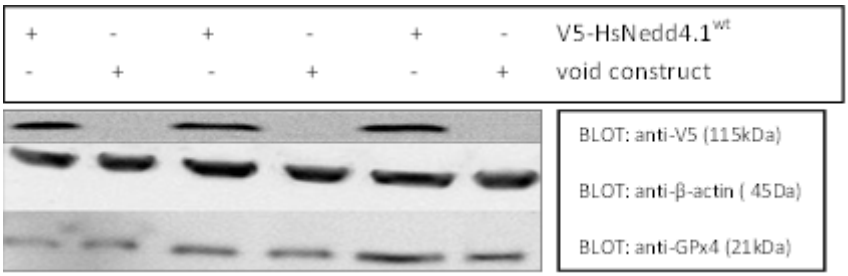

Figure 16. Effect of transfected Nedd4.1 on endogenous GPx4 turnover under unchallenged conditions. The experiment was performed in triplicate. Cells were transfected with V5-tagged Nedd4.1 or empty vector, as indicated, for 24 hours. After cell lysis, WB analysis was performed using the indicated anti-B-actin, anti-GPx4 and anti-V5 antibodies.

Next, we investigated whether Nedd4.1 affects GPx4 turnover under conditions of 'destabilization' of the peroxidase, such as those obtained by treating cells with compounds inducing ferroptosis, (e.g. GSH depletion or direct GPx4 inactivation by FIN II class of compounds) (65).

4.3 Setting up of the model of ferroptosis by glutathione depletion in HEK 293T cells

To induce GSH depletion, we used a combination of buthionine sulfoximine (BSO), a known inhibitor of gamma-glutamyl-cysteine-synthetase (78), the enzyme involved in GSH biosynthesis and diethyl maleate (DEM), which is involved in GSH alkylation (79). By the Tietze assay, we found that treatment of cells by these two compounds brings to a complete decline of total glutathione in 180 min (76) (Fig. 17A), which coincided with the onset of lipid peroxidation, cell death and morphological change (Fig. 17A-B-C)

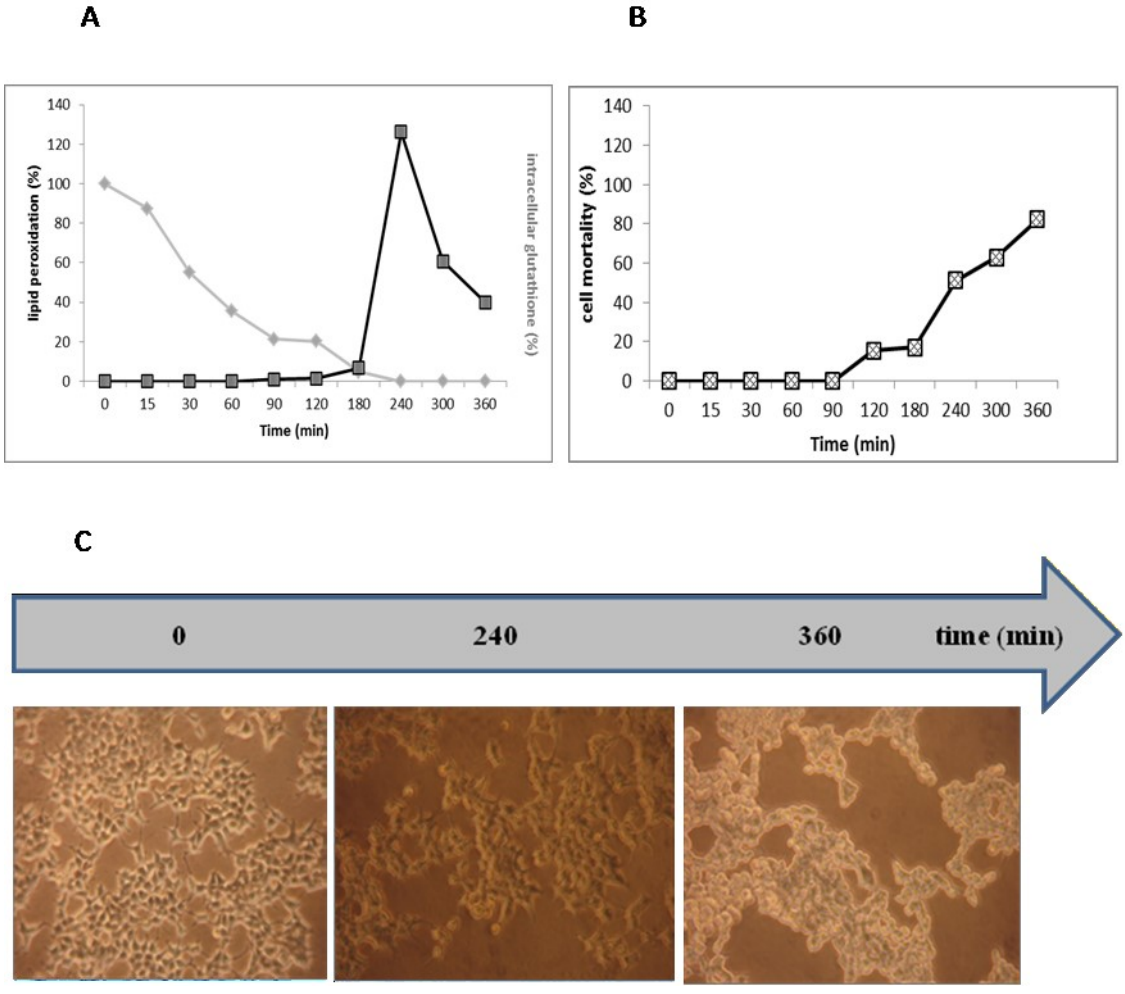

Figure 17. Effect of BSO and DEM treatment in HEK293T cells. Glutathione content (A) and lipid peroxidation (A), vitality (B) and morphology (C) were detected. Cells were treated by 5mM BSO and 500µM DEM for the time indicated. Total glutathione was measured by the Tietze method(76), lipid peroxidation by the fluorescent probe Bodipy, and cell vitality by the Alamar

blue assay (80). In C is reported the image of cells by an inverse optical microscope at the indicated time after BSO and DEM treatment.

Cell death was prevented by alpha-tocopherol and deferoxamine (Fig. 18A-B), thus confirming that ferroptosis, which impinge on GPx4, was indeed the subroutine of cell death taking place in our cells following GSH depletion by BSO and DEM.

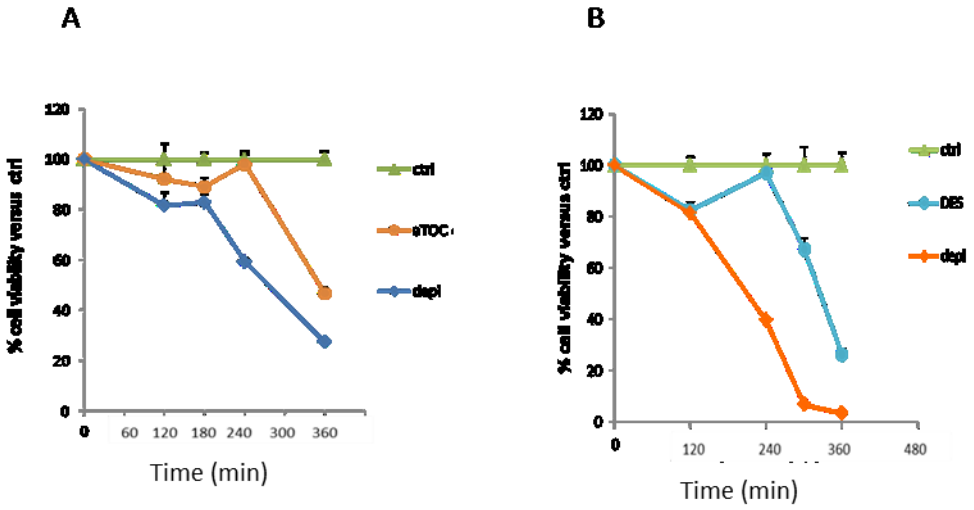

Figure 18. Effect of alpha tocopherol and deferoxamine on vitality of glutathione-depleted cells. HEK 293T control cells were challenged by BSO and DEM as in fig. 17. 400µM alpha tocopnerol (A) or 400µM deferoxamine (B) was added in the indicated samples. Vitality by Amar blue was measured at the indicated time and the results expressed as % versus control. Note that both compounds extend cell vitality

4.4 Glutathione depletion induces decrease of GPx4 in the cytosol, which is not affected by Nedd4.1 overexpression or proteasome inhibition by MG132

Next, we addressed the behavior of cytosolic GPx4 in terms of both, specific activity and protein amount, using the model of glutathione depletion leading to ferroptosis just set up. To this end, following glutathione depletion by BSO and DEM, GPx4 specific activity and protein were measured in the cytosolic fraction of cells. GPx4 activity was measured by the classic coupled spectrophotometric assay (see Methods), where GSH oxidation by the peroxidase is coupled to NADPH oxidation by the ancillary enzyme glutathione reductase. In this assay, specificity is granted by using the specific GPx4 substrate, phosphatidyl choline (PCOOH). As indicated in Fig. 19A, GPx4 specific activity decreased in the cytosol starting from 180 min following GSH depletion by combinated BSO and DEM treatment. This time remarkably coincides with total GSH depletion (grey line in Fig. 17A). Western blot analysis by the specific GPx4 antibody shows that decreased specific activity is accompanied with a parallel protein depletion from the cytosol (Fig. 19B).

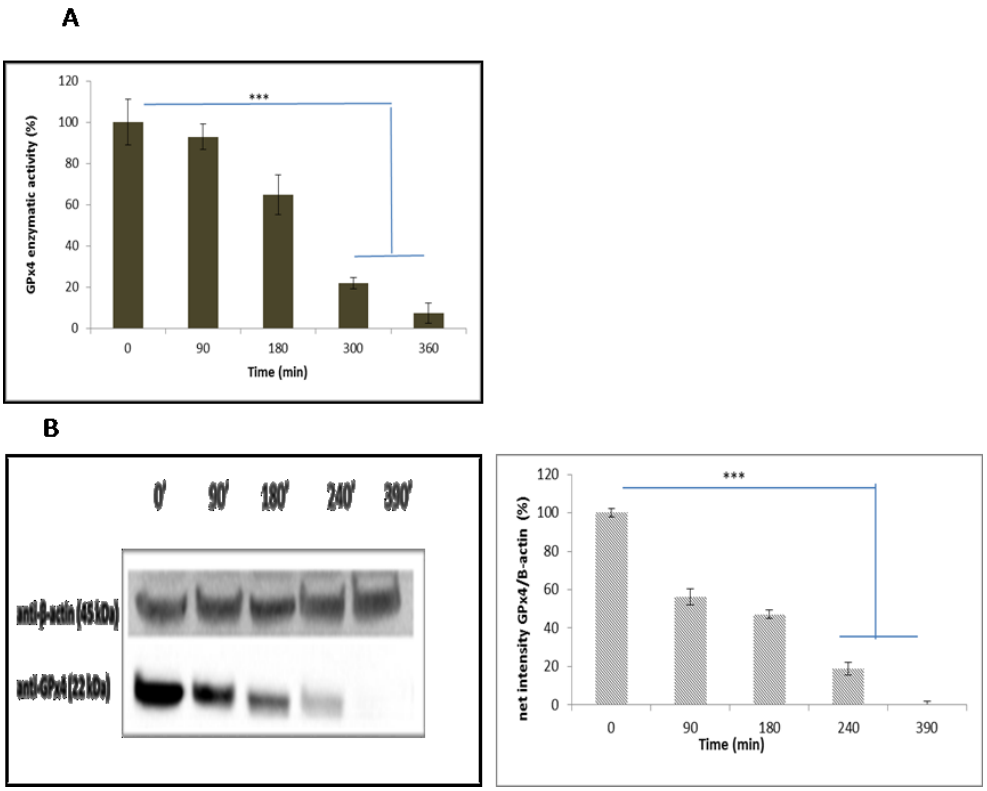

Figure 19. Effect of Glutathione depletion on cytosolic GPx4 specific activity and protein content. HEK293T cells were treated by BSO and DEM as indicated in Fig. 17 and Methods. At the indicated time cells were collected and cytosol was prepared. On the cytosolic fraction (A) GPx4 specific activity measurement and (B) western blot analysis were performed. For activity measurement, the specific substrate PCOOH was used. Total protein content in the cytosol was measured by Lowry method (75). 50 µg of total protein were loaded on SDS-PAGE and blotted on nitrocellulose for Western blot analysis. Home-made anti-GPx4 antibody or commercially available anti beta actin antibodies were used. See Methods for details.

Yet, Nedd4.1 overexpression did not accelerate cytosolic decrease of both GPx4 specific activity and protein amount induced by GSH depletion (Fig. 20A and 20B respectively). In addition, the proteasome inhibitor MG132 did not prevent the GPx4 depletion observed in this experimental setting (Fig. 21).

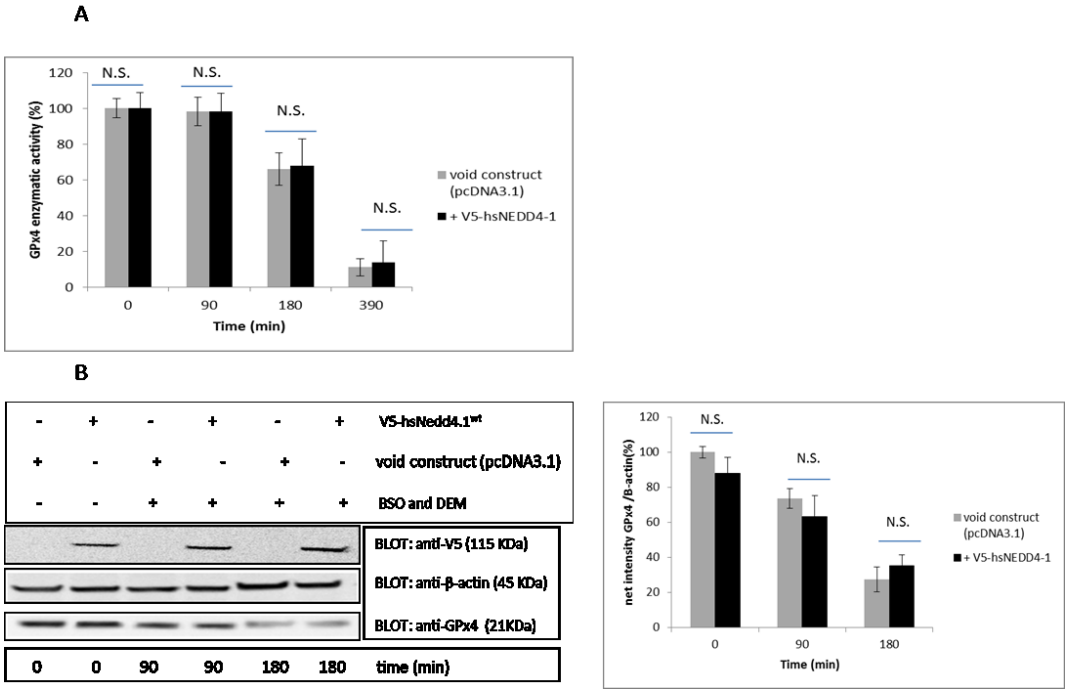

Figure 20. Effect of Nedd4.1 overexpression on cytosolic GPx4 specific activity/protein decrement following GSH depletion in HEK293T cells. Cells were transfected with expression construct for V5-Nedd4.1 (see Fig.13 and Methods). After 36 hours, cells were treated by BSO and DEM as indicated in Fig. 17. At the indicated time cells were collected and cytosol was prepared as described in Methods. Following protein measurements, sample were analyzed for (A) GPx4 specific activity and (B) GPx4 specific content by western blotting. Western blot was also

developed by anti-V5 antibody, to assess Nedd4.1 transfection, and anti-β-actin antibody, for quantification, as reported in the right panel

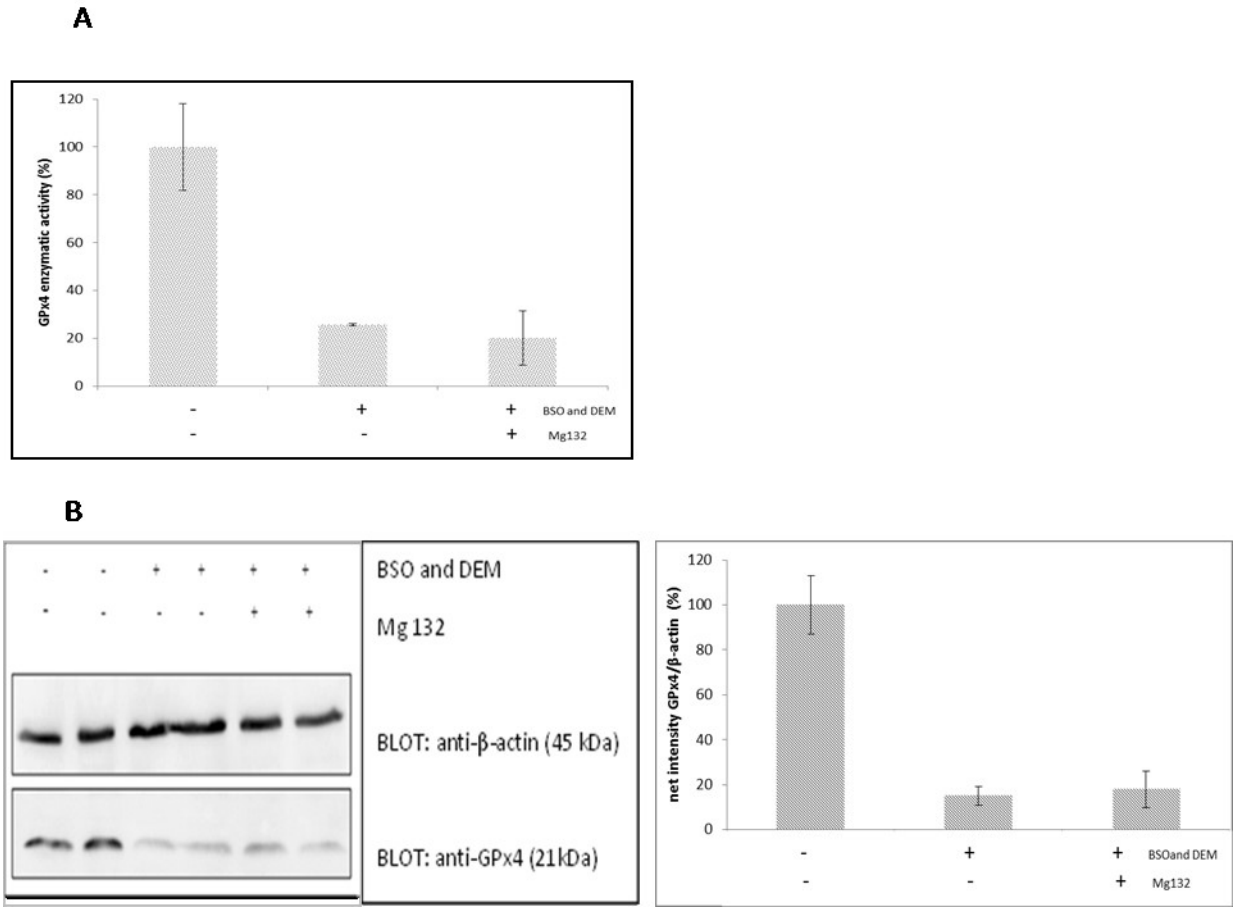

Figure 21. Effect of MG 132 on cytosolic GPx4 specific activity/protein decrement following GSH depletion in HEK293T cells. Cells were treated with BSO and DEM in the presence of 20 µM MG132 for 5 hours, when cells collected and cytosol prepared as described in Methods. Following protein measurements, sample were analyzed for (A) GPx specific activity and (B) specific GPx4 content by western blotting. The experiment was performed three times, with similar results.

4.5 1S,3R-RSL3 treatment in cells inactivates GPx4: inactive GPx4 remains in the cytoplasm and its clearance is not modified by Nedd4.1

We therefore addressed whether Nedd4 activity is involved in clearing up GPx4 another mechanism leading to GPx4 destabilization, such as that relying on FIN II class of compounds, e.g. 1S,3R-RSL3. For this purposes HEK293T cells were treated with 1S,3R-RSL3 and the behavior of cytosolic GPx4 in terms of both, specific activity and protein amount was addressed. As indicated in Fig. 22 treatment of HEK293T cells by 1S,3R-RSL3 (but not by the inactive isomer 1R,3R-RSL3), induced a fast decrease of GPx4 specific activity in the cytosol (Fig. 22A). Differently from BSO and DEM-treated cells however, 1S,3R-RSL3 treatment did not affect the concentration of the protein in the cytosol (Fig. 22B), indicating that the inactive form of GPx4 remained in the cytosol. Yet, we were unable to detect any further clearance of GPx4 upon Nedd4.1 overexpression (fig. 23).

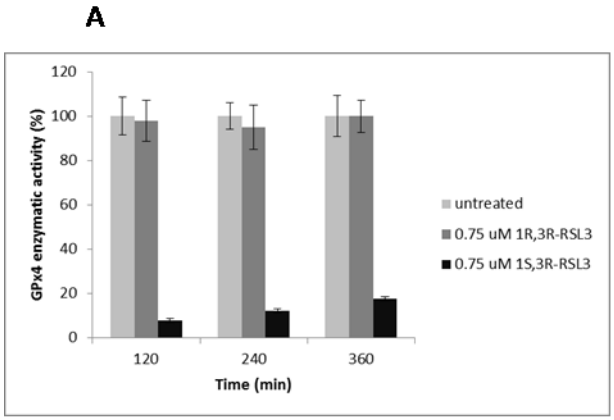

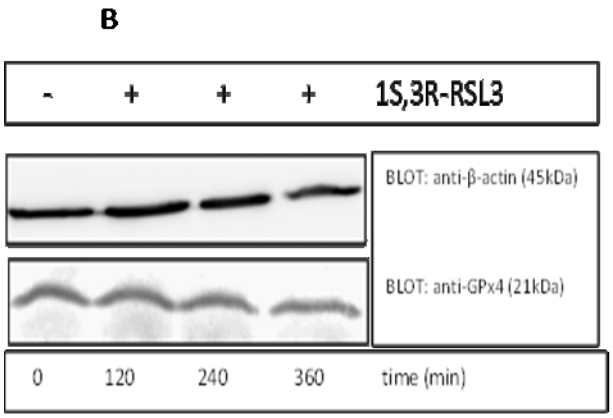

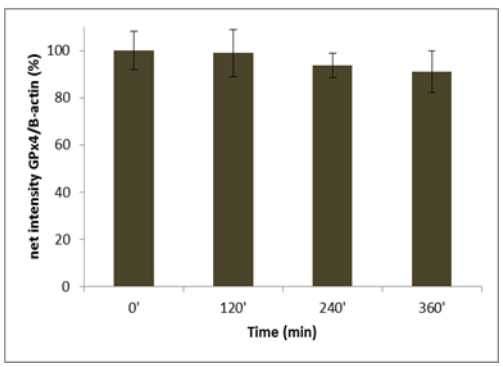

Figure 22. Effect of RSL3 on GPx4 specific activity and protein content in the cytosol of HEK293T cells. Cells were treated with 0.75 µM 1S,3R-RSL3 or 0.75 µM 1R,3R-RSL3 for the indicated time. Cytosol was prepared as described in Methods. Following protein measurements, sample were analyzed for (A) GPx specific activity and (B) specific GPx4 content by western blotting. Note that the isomer 1R,3R-RSL3 is unable to induce GPx4 inactivation, indicating that the reaction is stereospecific and that differently from the GSH depletion model, inactive GPx4 remains in the cytosol.

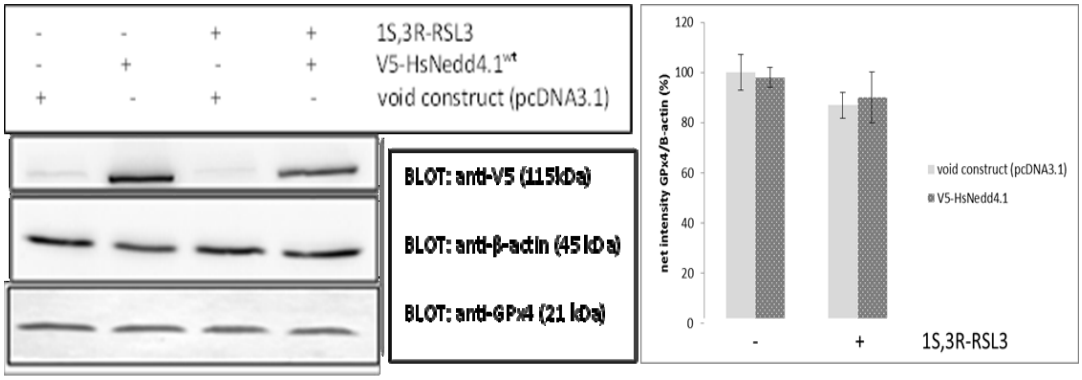

Figure 23. Effect of Nedd4.1 overexpression on cytosolic GPx4 protein following 1S,3R-RSL3 treatment in HEK293T cells. Cells were transfected with expression construct for V5-Nedd4.1 or with empty vector pcDNA3.1 (Fig. 13 and Methods) After 36 hours, cells were treated by 1S,3R-RSL3 as indicated in Fig.22. After 2 hours, cells were collected and cytosol was prepared as described in Methods. Following protein measurements, sample were analyzed GPx4 specific content by western blotting. Western blot was also developed by anti-V5 antibody, to assess Nedd4 transfection, and anti-β-actin antibody, for quantification, as reported in the right panel

4.6 GSH depletion induces GPx4 translocation on the membranes.

In the attempt of clarifying the mechanism underlying GPx4 decrement in the cytosol in our model of ferroptosis by GSH depletion, we analyzed GPx4 content in the residual pellet obtained after centrifugation yielding the cytosolic fraction. Surprisingly, we found that the GPx4 appears in this membrane fraction as a function of time following BSO and DEM treatment, while disappearing from

the cytosol (Fig. 24A and B). Nevertheless this membrane GPx4 is not reactive with anti-Ub antibody, suggesting that Ub is not involved in the observed translocation (Fig. 24C).

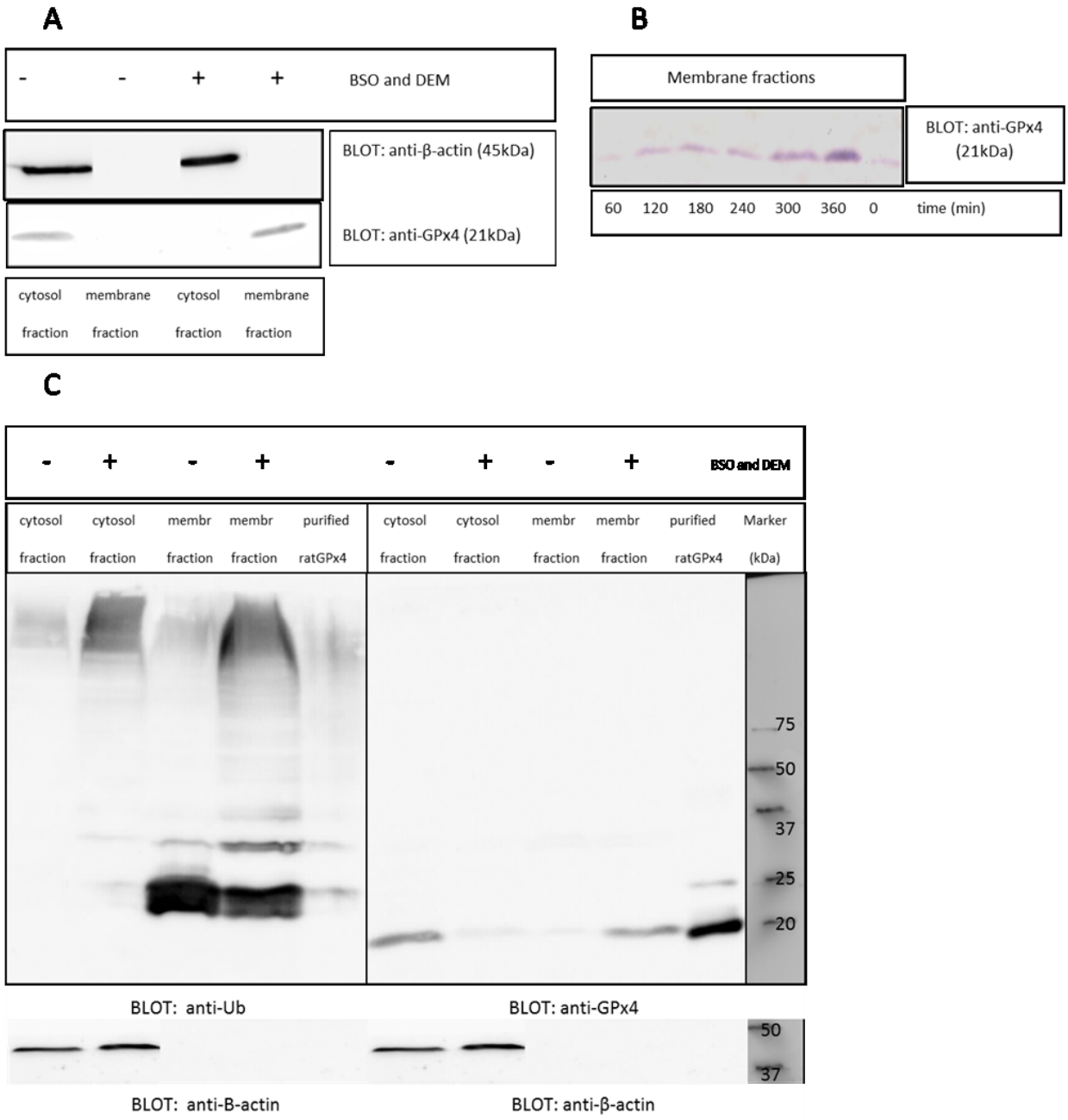

Figure 24. Analysis of the pellet from GSH-depleted cells. HEK 293T cells were treated by BSO and DEM as indicated in Fig.17 and Methods. (A) After 360 min or (B) at the indicated time, cells were collected and cytosol was prepared. Western blot analysis with anti GPx4 antibody (A and B), or Anti-Ub antibody (C) was performed. In the indicated fraction, total protein content was measured by the Lowry method (75). See Methods for details. All together results indicate that after 360 min cytosolic GPx4 is translocated to the membranes in a non-ubiquitylated form.

The obtained results, therefore, suggest that GSH depletion, differently from 1S, 3R-RSL3 treatment, induces the translocation of GPx4 from cytosol to membranes by a process that does not involve Ub. Thus, apparently, in the absence of GSH, GPx4 affinity for membrane is increased.

This finding has been indeed confirmed by Surface Plasmon Resonance (SPR) experiments, where extruded liposomes containing DOPC:TOCL (80:20 or 50:50) were immobilized on a chip and the interaction with purified GPx4 was measured in the presence or absence of high ionic strength and GSH (fig. 25). The interaction between GPx4 and the phospholipid bilayer was measured as equilibrium dissociation constant (K_D). Results indicate that the K_D for the reaction between GPx4 and the phospholipid bilayer, which increases in the presence of high ionic strength (KCl), is further significantly increased in the presence of GSH. Thus the affinity of GPx4 for the phospholipid bilayer of liposomes is increased by low ionic strength and absence of GSH.

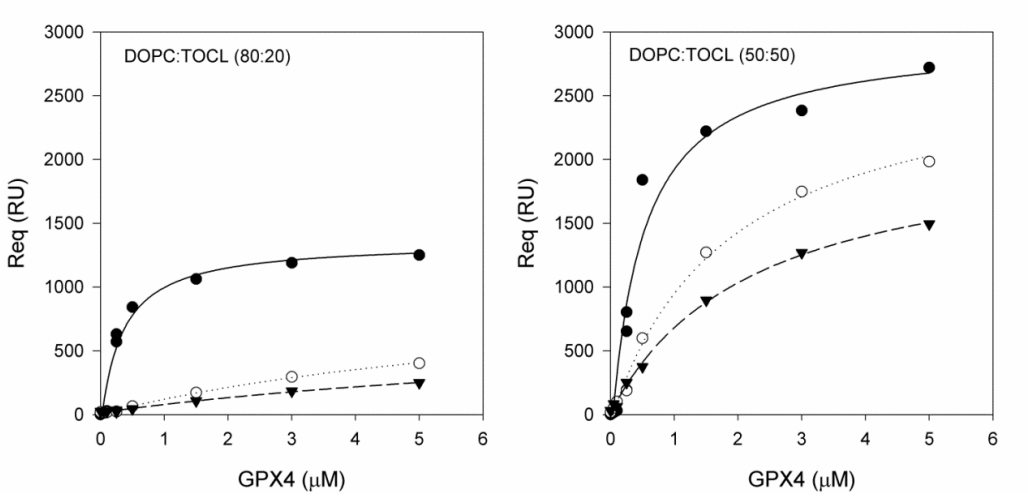

Bilayer		K_D (μM)	R_{max} (RU)
DOPC:TOCL (80:20)	Tris	0.5±0.2	1708±153
DOPC:TOCL (80:20)	Tris/KCl	4.6±0.9	812±81
DOPC:TOCL (80:20)	Tris/KCl/GSH	8±2	640±110
DOPC:TOCL (50:50)	Tris	0.3±0.1	3509±389
DOPC:TOCL (50:50)	Tris/KCl	1.6±0.3	2808±160
DOPC:TOCL (50:50)	Tris/KCl/GSH	2.1±0.3	2135±105

Figure 25. Effect of ionic strength and GSH on the interaction between GP^x4 and TOCL liposomes and calculated dissociation constant. In the top panel the sensorgrams of the binding of GPx4 to a bilayer composed of DOPC and TOCL is reported. The sensograms are produced by subtracting the signal from lanes containing DOPC from lanes containing DOPC:TOCL 1:1. Results, therefore, refer specifically to the interaction between GPx4 and TOCL. Equilibrium bindings (R_{eq}) were measured for various concentrations of GPx4 on DOPC: TOCL (80:20 and 50:50). The running buffer was : 25mM TRIS-HCl, pH 7.4 (●); running buffer, 150mM KCl, pH 7.4 (○); and running buffer, 150mM KCl 5mM GSH, pH 7.4 (▼).From the equilibrium bindings (Req) the equilibrium dissociation constant (KD) were calculated by fitting the equation:
Req= Rmax ·A/(K_D+A) where A is the GPx4 concentration and Rmax is the maximum value of the biosensor signal. Similar results were obtained for phosphatidyl inositol, phosphatidyl ethanolamine and phosphatidic acid/DOPC liposomes, all interacting with GPx4 less than TOCL.

Furthermore, a combined approach of molecular docking and molecular dynamic simulations, made in collaboration with G. Cozza, research fellow at the Department of Molecular Medicine at the University of Padua, shows an optimal juxtaposition between GPx4 and the membrane, apparently driven by the electrostatic network in the cationic area of GPx4, located on the surface of GPx4, close to the catalytic pocket (see paragraph in the introduction). This gives, indeed, a rationale for the sensitivity to ionic strength of the binding between GPx4 and membranes observed by SPR (see above and Fig. 25). Interestingly, this

optimal electrostatic interaction between GPx4 and the membrane allows the hydroperoxy group (simulated both in position 9 and 13 in the esterified fatty acids) to be specifically addressed toward the redox-active selenium in the catalytic pocket of GPx4 (cartoon on Fig. 26). Furthermore, molecular dynamic analysis indicates that the tight interaction between GPx4 and membrane hydroperoxides becomes less strong upon reduction of the hydroperoxide to corresponding alcohol by GPx4. This allows GSH to access the oxidized selenium moiety, thus producing the mixed selenodisufide. Presence of selenodisulfide in GPx4 further weakens the interaction with the phospholipid bilayer. In addition, the second GSH molecule required for the complete reduction of the peroxidase, is oriented toward the mixed selenodisulfide by some of the aminoacids, located in the basic zone, which eventually, once bound to the second GSH, completely loose the contact with the polar head of the phospholipid.

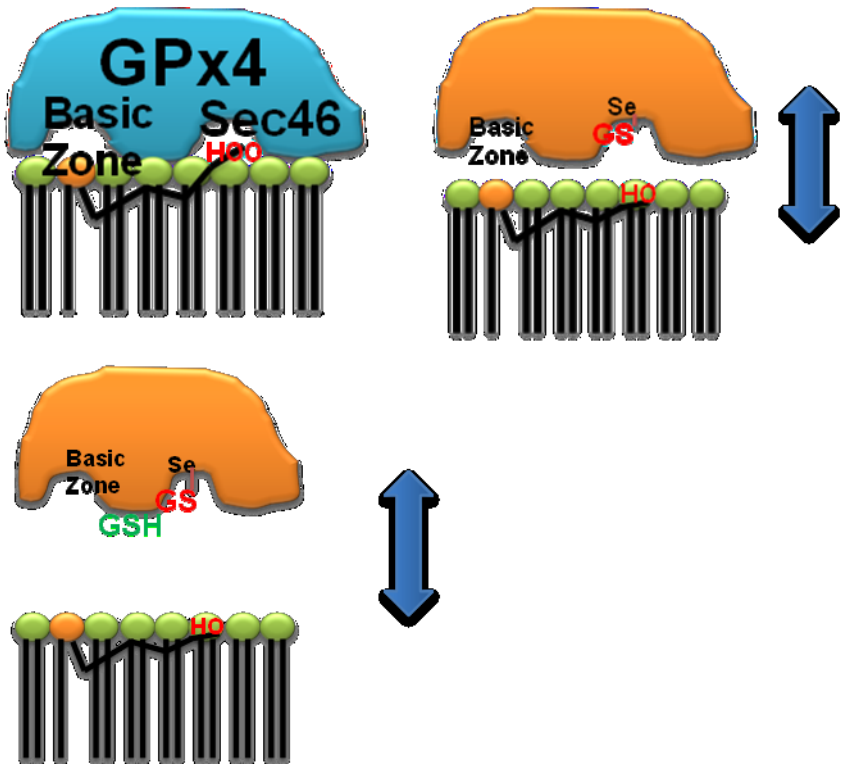

Figure 26. Cartoon representation of the molecular docking and MD simulation of Interaction between GPx4 and membrane phospholipid. The molecular dynamics simulation showed that after just 50ns the hydroperoxide group posed in the core of the membrane on the fatty acid

esterified in the phospholipid moves up, becoming close to lipid water interface, and becoming solvent exposed. The optimal interaction of GPx4 with the polar head of the phospholipid allows the contact of the hydoperoxide with the flat surface containing the redox-active selenium (top left cartoon). Following reduction of the hydroperoxides an initial destabilization of the contact occurs allowing the first molecule of GSH to interact with oxidized selenium forming a mixed selenodisulfide. This further weakens the interaction with the phospholipid bilayer (Top right cartoon). The second GSH molecule is oriented toward the mixed selenodisulfide by some aminoacid the basic zone, which eventually, once bound to the second GSH completely loose the contact with the polar head of the phospholipid. As a result, GPx4 lose the contact with the membrane (lower cartoon).

5 DISCUSSION

GPx4 and/or its substrate GSH are emerging as major determinants of cell fate (i.e. regulating the balance between proliferation and death), at least in live animals and in some cultured cells (57) . Reverse genetics studies indicate that all the tissues where GPx4 was in so far silenced (e.g. brain (46), kidney (81), liver (82), skin (83)), undergo degeneration. Understanding therefore GPx4 turnover is a crucial issue.

We addressed whether ubiquitylation by Nedd4 isoforms and subsequent proteasomal degradation, could have a role in GPx4 turnover. The work was inspired by a conserved LPXY motif observed in the C-terminal end of GPx4 (Fig. 11), which is in a canonical position for many Nedd4 isoforms substrates (73,84). Unexpectedly, obtained data did not indicate that GPx4 is a Nedd4 substrate. Indeed *in vivo* transfection experiments showed that *Hs*GPx4 and *Hs*Nedd4.1, being co-immunoprecipitated, bind each other, and the same holds true for *Hs*GPx4 and *Hs*Nedd4.2. Furthermore, apparently, binding relies, at least in part, on GPx4 LPXY C-terminal motif, in fact a weaker signal for Nedd4.1 is obtained in the GPx4 co-immunoprecipitate following co-transfection with *Hs*GPx4 carrying the LPHA C-terminal motif mutated into LAHA (Fig.13). Yet, in the road to demonstrate occurrence of GPx4 ubiquitylation by the Nedd4 isoforms we stepped into some problems that questioned the specificity of the ubiquitylation reaction carried by the adopted *in vivo* assay. This was indeed disappointing since this assay is indeed a 'golden standard' for detecting Nedd4 isoforms substrates (73). Analysis of the 'pre-cleaned' GPx4 co-immunoprecipitate from Nedd4.1 or Nedd4.2 and GPx4 co-transfected cells reveals indeed a smear positive to the anti-Ub antibodies (Fig. 14), but whether the Nedd4 isoforms and GPx4 are involved in the observed signal, as E3 ligase and substrate respectively, was difficult to prove. The ubiquitylation pattern observed in the GPx4 co-immunoprecipitate of cells co-trasfected as above is not affected if an inactive mutant of the catalytic Cys of Nedd4.1 or Nedd4.2 (Nedd4.1 $^{Cys/Ser}$ or Nedd4.2 $^{Cys/Ser}$) is used in place of the corresponding wild type. Thus apparently, in our experimental setting, other ubiquitylating enzymes, distinct from the transfected

Nedd4 isoforms, are responsible for the observed ubiquitylation signal. Furthermore whether the ubiquitylated protein is GPx4 or other proteins are the Ub targets, could not be unequivocally established, despite the fact that GPx4 is present in the co-immunoprecipitate (Fig. 14). In the attempt of improving specificity, we manipulated the pre-cleaning procedure of the co-immunoprecipitate by increasing the concentration of SDS, which should improve the purity by discarding loosely bound proteins. Unfortunately, the obtained results were not encouraging at all. Indeed, the ubiquitylation signals disappeared from all the samples, including our positive control (not shown).

We therefore addressed the initial question, i.e. whether GPx4 is ubiquitylated by any of the Nedd4 isoforms, by a cell-free *in vitro* ubiquitylation assay, which has the obvious advantage of lacking major cellular contaminants that may interfere with specific GPx4 ubiquitylation. By this means we could unequivocally exclude that rat purified GPx4 is ubiquitylated by recombinant Nedd4.1 (Fig. 15). Yet, the possibility that the purified GPx4 used for the *in vitro* assay was not a suitable substrate for ubiquitylation, differently from that in cells following a ferroptotic signal, was seen as a possible bias of the *in vitro* experiment. As a matter of fact, the GPx4 is reported to disappear following ferroptosis by western blot analysis (85). On this light, the observation that, in non-challenged cells, overexpressing Nedd4.1 does not affect endogenous GPx4 turnover (Fig. 16), was somehow expected. To overcome the above bias, we compared endogenous GPx4 activity and protein in cells undergoing ferroptosis while overespressing or not Nedd4.1.

Ferroptosis was induced by FINI or FINII compounds. Notably, in both the ferroptotic models GPx4 is a major target, FIN I acting on GPx4 indirectly (by depleting the electron donor for GPx4 catalytic activity on membrane phospholipid hydroperoxides) and FIN II acting by direct GPx4 modification.

Of the two models, that relying on FIN I compounds was exhaustively studied. Obtained results indicate that a combined BSO and DEM treatment in HEK293T cells induces a progressive total glutathione depletion, which is completed after 3 hours, exactly when lipid peroxidation and cell death start increasing (Figure 17). Interestingly, total glutathione depletion coincides with both, a decreased

GPx4 activity and protein in the cytosol (Fig 19). Yet, Nedd4.1 overexpression does not affect the time course of GPx4 decrease (Fig. 20), and, in addition, the proteasome inhibitor MG 132 fails to prevent it (Fig. 21). All together these data rule out the involvement of both, Nedd4 and the proteasome in GPx4 clearance following GSH depletion in HEK293T cells. Furthermore, results ruling-out any involvement of Nedd4.1 in GPx4 turnover in cells undergoing ferroptosis were also obtained by treating the same cell type with the FIN II compound 1S,2R RSL3. As demonstrated in Fig. 23, the amount of GPx4 in the cytosol is not affected by Nedd4.1 overexpression in 1S,3R-RSL3-treated cells. Notably however, while 1S,3R-RSL3 inactivates endogenous GPx4, the latter does not decrease as a protein, remaining detectable in the cytosol up to 6 hours, although in an inactive form (Fig. 22).

Intrigued by the observation that glutathione depletion leads to a decreased amount of endogenous GPx4 in the cytosol, independently from proteasome activity, we addressed the fate of the cytosolic protein. Surprisingly, the amount of GPx4 in the residual pellet from the centrifugation yielding the cytosol, increases as a function of time following BSO and DEM treatments (Fig. 24). This suggested that, upon GSH depletion, GPx4 is addressed to the membranous fraction of the cells. It is well known that ubiquitylation is also involved in addressing the protein to specific cell compartments (86–89), therefore we addressed whether membrane-linked GPx4 following GSH depletion was indeed ubiquitylated. Western blot analysis of the membrane fraction did not support this view (Fig. 24). We concluded therefore that it is GSH depletion *per se* that induces a translocation of GPx4 to the membrane.

The latter hypothesis was supported both by SPR studies, that showed that affinity of GPx4 for the phospholipid bilayer of liposomes containing TOCL is increased, besides by low ionic strength, by absence of GSH. In further support, came a combined docking and molecular dynamic approach. This approach, made in collaboration with Dr. G. Cozza, research fellow at our Department, was aimed to explore how the enzyme works on membranes during the catalytic cycle. It suggested that GPx4 binds to the polar head of membrane phospholipid by its basic zone adjacent to the catalytic site, and, upon oxidation, the

interaction with GSH releases the enzyme in the cytosol. As a matter of fact, in the second reductive step of the catalytic cycle, GSH is addressed to the catalytic moiety by some of the aminoacids of the basic zone binding the polar head of phospholipids. By binding to the enzyme, therefore, GSH displaces the phospholipid, moving the protein to the cytosol.

In conclusion our work, although showing a LPXY motif-dependent binding between both the Nedd4 isoforms and GPx4, fails to validate the hypothesis that GPx4 is ubiquitylated by these ligases, which appear indeed not involved in GPx4 turnover. Yet, the observation that GPx4 translocates to membrane under GSH depletion opens interesting perspectives in the understanding of the mechanism underlying the action of GPx4 on biological membranes.

REFERENCES

1. Hochstein P, Ernster L. ADP-Activated Lipid Peroxidation Coupled To The TPNH Oxidase System Of Microsomes. Biochem Biophys Res Commun. 1963;388–94.

2. McCay P, Gibson B, Kuo-Lan F, Roger H. Effect of glutathione peroxidase activity on lipid peroxidation in biological membranes. BBA-lipid and lipid metabolism. 1976;459–68.

3. Gibson DD, Hornbrook KR, McCay PB. Glutathione-dependent inhibition of lipid peroxidation by a soluble, heat-labile factor in animal tissues. Biochem Biophys Acta. 1980;572–82.

4. Ursini F, Maiorino M, Valente M., Ferri L, Gregolin C. Purification from pig liver of a protein which protects liposomes and biomembranes from peroxidative degradation and exhibits glutathione peroxidase activity on phosphatidylcholine hydroperoxides. Biohim Biophys Acta. 1982 Feb;197–211.

5. Ursini F, Maiorino M, Gregolin C. The selenoenzyme phospholipid hydroperoxide glutathione peroxidase. Biochimica et Biophysica Acta (BBA) - Biomembranes. 1985th ed. :62–70.

6. Thomas JP, Geiger PG, Maiorino M, Ursini F, Girotti AW. Enzymatic reduction of phospholipid and cholesterol hydroperoxides in artificial bilayers and lipoproteins. Biochim Biophys Acta. 1990;252–60.

7. Thomas JP, Maiorino M, Ursini F, Girotti AW. Protective action of phospholipid hydroperoxide glutathione peroxidase against membrane-damaging lipid peroxidation. In situ reduction of phospholipid and cholesterol hydroperoxides. J Biol Chem. 1990;265(1):454–61.

8. Schuckelt R, Brigelius-Flohé R, Maiorino M, Roveri A, Reumkens J, Strabburger W, et al. Phospholipid Hydroperoxide Glutathione Peroxidase is a Seleno-Enzyme Distinct from the Classical Glutathione Peroxidase as Evident from Cdna and Amino Acid Sequencing. Free radical research and communication.

9. Brigelius-Flohé R, Aumann K-D, Blöcker H, Gross G, Kiess M, Klöppel KD, et al. Phospholipid-hydroperoxide glutathione peroxidase. Genomic DNA, cDNA, and deduced amino acid sequence. J Biol Chem. 1994;269(10):7342–8.

10. Gladyshev VN, Arner ES, Berry MJ, Brigelius-Flohé R, Bruford EA, Burk RF, et al. Selennoprotein Gene Nomenclature. J Biol Chem. 2016;

11. Brigelius-Flohé R, Maiorino M. Glutathione peroxidases. Biochim Biophys Acta BBA - Gen Subj. 2013 May;1830(5):3289–303.

12. Toppo S, Vanin S, Bosello V, Tosatto SCE. Evolutionary and Structural Insights Into the Multifaceted Glutathione Peroxidase (Gpx) Superfamily. Antioxid Redox Signal. 2008 Sep;10(9):1501–14.

13. Maiorino M, Roveri A, Benazzi L, Bosello V, Mauri P, Toppo S, et al. Functional interaction of phospholipid hydroperoxide glutathione peroxidase with sperm mitochondrion associated cysteine rich protein disclosed teh adjacent cysteine motif as a substrate of the selenoperoxidase. JBiolChem. 280th ed. 2005;38395–402.

14. Maiorino M, Bosello V, Cozza G, Miotto G, Roveri A, Toppo S. Understanding mammalian glutathione peroxidase 7 in the light of its homologs. Free Radic Biol Med. 2015;352–60.

15. Epp R, Ladenstein A, Wendel E. The refined structure of the selenoenzyme glutathione peroxidase at 0.2 nm resolution. JBiochem. 1983;51–69.

16. Martin JL. Thioredoxin—a fold for all reasons. Structure. 1995;3(3):245–50.

17. Ursini F, Maiorino M, Brigelius-Flohé R, Aumann KD, Roveri A, Schomburg D, et al. Diversity of glutathione peroxidases. Methods Enzymol. 252nd ed. 1995;38–53.

18. Tosatto S. The catalytic site of Glutathione Peroxidase. Antioxidats & Redox Signalling. 2008;1515–26.

19. Toppo S, Flohé L, Ursini F, Vanin S, Maiorino M. Catalytic mechanisms and specificities of glutathione peroxidases: Variations of a basic scheme. Biochim Biophys Acta BBA - Gen Subj. 2009 Nov;1790(11):1486–500.

20. Maiorino M, Gregolin C, Ursini F. Phospholipd hydroperoxide glutathione proxidase. Methods in Enzymology. 1990;448–57.

21. Orian L, Mauri P, Roveri A, Toppo S, Benazzi L, Bosello V, et al. Selenocysteine oxidtion in glutathione peroxidase an MS-supported quantum mechanics study. Free Radic Biol Med. 2015;1–14.

22. Imai H, Hirao F, Sakamoto T, Sekine K, Mizukura Y, Saito M, et al. Early embryonic lethality caused by targeted disruption of the mouse PHGPx gene. Biochem Biophys Res Commun. 2003 May;305(2):278–86.

23. Yoo S-E, Chen L, Na R, Liu Y, Rios C, Van Remmen H, et al. Gpx4 ablation in adult mice results in a lethal phenotype accompanied by neuronal loss in brain. Free Radic Biol Med. 2012 May;52(9):1820–7.

24. Schnurr K, Belkner J, Ursini F, Schewe T, Kühn H. The selenoenzyme phospholipid hydroperoxide glutathione peroxidase controls the activity of the 15-lipoxygenase with complex substrates and preserves the specificity of the oxygenation products. J Biol Chem. 1996;271(9):4653–8.

25. Huang H-S, Chen C-J, Suzuki H, Yamamoto S, Chang W-C. Inhibitory effect of phospholipid hydroperoxide glutathione peroxidase on the activity of lipoxygenases and cyclooxygenases☆. Prostaglandins Other Lipid Mediat. 1999;58(2):65–75.

26. Schneider M, Forster H., Boersma A., Seiler A., Wehnes H., Sinowatz F., et al. Mitochondrial glutathione peroxidase 4 disruption causes male infertility. Faseb J. 2009;3233–42.

27. Brault C, Lévy P, Duponchel S, Michelet M, Sallé A, Pécheur E-I, et al. Glutathione peroxidase 4 is reversibly induced by HCV to control lipid peroxidation and to increase virion infectivity. Gut. 2016 Jan;65(1):144–54.

28. Pushpa-Rekha TR, Burdsall AL, Oleksa LM, Chisolm GM, Driscoll DM. Rat phospholipid-hydroperoxide glutathione peroxidase cDNA cloning and identification of multiple transcription and translation start sites. J Biol Chem. 1995;270(45):26993–9.

29. Arai M, Imai H, Sumi D, Imanaka T, Takano T, Chiba N, et al. Import into mitochondria of phospholipid hydroperoxide glutathione peroxidase requires a leader sequence. Biochem Biophys Res Commun. 1996;227(2):433–9.

30. Pfeifer H, Conrad M, Roethlein D, Kyriakopoulos A, Brielmeier M, Bornkamm GW, et al. Identification of a specific sperm nuclei selenoenzyme necessary for protamine thiol cross-linking during sperm maturation. Faseb J. 2001;1236–8.

31. Maiorino M, Scapin M, Ursini F, Biasolo M, Bosello V, Flohè L. Distinct promoters determine alternative transcription of gpx-4 into phospholipid-hydroperoxides glutathione peroxidase variants. JBiolChem. 2003;34286–90.

32. Maiorino M, Roveri A, Ursini F. Phospholipid hydroperoxide glutathione peroxide is the major selenoperoxidase in nuclei and mitochondrial of rat testis. From Basic Science To Medicine. 1993;412–8.

33. Liang H, Yoo S-E, Na R, Walter CA, Richardson A, Ran Q. Short form glutathione peroxidase 4 is the essential isoform required for survival and somatic mitochondrial functions. J Biol Chem. 284th ed. 2009;30836–44.

34. Smith AC, Mears AJ, Bunker R, Ahmed A, MacKenzie M, Schwartzentruber JA, et al. Mutations in the enzyme glutathione peroxidase 4 cause

Sedaghatian-type spondylometaphyseal dysplasia. J Med Genet. 2014 Jul;51(7):470–4.

35. Imai H, Hakkaku N, Nagakawa Y. Depletion of Selenoprotein GPx4 in Spermatocytes Causes Male Infertility in Mice. The journal of Biological Chemistry. 2009;32522–32.

36. Wallace E, Calvin HI, Ploetz K, Cooper GW. Functional and developmental studies on the role of Selenium in spermatogenesis. 1987;

37. Conrad M, Moreno SG, Sinowatz F, Ursini F, Kolle S, Roveri A, et al. The Nuclear Form of Phospholipid Hydroperoxide Glutathione Peroxidase Is a Protein Thiol Peroxidase Contributing to Sperm Chromatin Stability. Mol Cell Biol. 2005 Sep 1;25(17):7637–44.

38. Ursini F, Heim S, Kiess M, Maiorino M, Roveri A, Wissing J, et al. Dual Function of the Selenoprotein PHGPx During Sperm Maturation. Science. 1999 Aug 27;285(5432):1393–6.

39. Shalgi R, Seligman J, Kosower NS. Dynamics of the thiol status of rat spermatozoa during maturation: analysis with the florescent labelling agent monobromobibame. Biol Reprod. 1998;1037–45.

40. Dixon SJ, Lemberg KM, Lamprecht MR, Skouta R, Zaitsev EM, Gleason CE, et al. Ferroptosis: An Iron-Dependent Form of Nonapoptotic Cell Death. Cell. 2012 May;149(5):1060–72.

41. Maiorino M, Coassin M, Roveri A, Ursini F. Microsomal lipid peroxidation: effect of vitamin E and its functional interaction with phospholipid hydroperoxide glutathione peroxidase. Lipids. 24th ed. 1989;721–6.

42. Ursini F, Maiorino M, Hochstein P, Ernster L. Microsomal lipid peroxidation: mechanisms of initiation. The role of iron and iron chelators. Free Radic Biol Med. 6th ed. :31–6.

43. Yamamoto S. Mammalian lipoxygenase: molecular structures and functions. Biochem Biophys Acta. 1128th ed. 1992;117–31.

44. Schewe T, Halangk W, Hiebsch C, Rapoport SM. A lipoxygenase in rabbit reticulocytes which attacks phospholipids and intact mitochondria. FEBS Lett. 1975;60(1):149–52.

45. Kuhn H, Belkner J, Wiesner R, Brash AR. Oxygenation of biological membranes by the pure reticulocyte lipoxygenase. J Biol Chem. 1990;265(30):18351–61.

46. Seiler A, Schneider M, Forster H., Roth SR, Wirth EK, Culmsee C, et al. Glutathione Peroxidase 4 Senses and Translates oxidative stress into 12 15

Lipoxygenase Dependent- and AIF-mediated cell death. Cell Metabolism. 8th ed. 2008;237–48.

47. Brutsch S, Wang CC. LL, Kuhn H, Borchet A. Expression of inactive glutathione peroxidase 4 leads to embryonic lethality, and inactivation of the Alox15 gene does not rescue such knock-in mice. Antioxidants & Redox Signaling. 2015;281–93.

48. Brutsch SH, Rademacher M, Roth SR, Muller K, Eder S, Viertel D, et al. Male subfertility induced by heterozygous expression of catalytically inactive glutathione peroxidase 4 is rescued in vivo by systemic inactivation of the Alox15 gene. J Biol Chem. 2016 Sep 15;jbc.M116.738930.

49. Schilstra MJ, Veldink GA, Verhagen J, Vliegenthart JF. Effect of lipid hydroperoxide on lipoxygenase kinetics. Biochemistry. 31st ed. 1992;7692–9.

50. Ivanov I, Kuhn H, Heydeck D. Structural and functional biology or arachidonic acId 15-lipoxygenase-1 (ALOX-15). Gene. 2015;

51. Dixon SJ, Stockwell BR. The role of iron and reactive oxygen species in cell death. Nature chemical biology. 2014;9–17.

52. Vigil D, Cherfils J, Rossman KL, Der CJ. Ras superfamily GEFs and GAPs: validated and tractable targets for cancer therapy? Nat Rev Cancer. 2010 Dec;10(12):842–57.

53. Dolma S, Lessnick SL, Hahn WC, Stockwell BR. Identification of genotype-selective antitumor agents using synthetic lethal chemical screening in engineered human tumor cells. Cancer Cell. 2003;3(3):285–96.

54. Schott C, Graab U, Cuvelier N, Hahn H, Fulda S. Oncogenic RAS Mutants Confer Resistance of RMS13 Rhabdomyosarcoma Cells to Oxidative Stress-Induced Ferroptotic Cell Death. Front Oncol [Internet]. 2015 Jun 22 [cited 2016 Sep 20];5. Available from: http://journal.frontiersin.org/Article/10.3389/fonc.2015.00131/abstract

55. Friedmann Angeli JP, Schneider M, Proneth B, Tyurina YY, Tyurin VA, Hammond VJ, et al. Inactivation of the ferroptosis regulator Gpx4 triggers acute renal failure in mice. Nat Cell Biol. 2014 Nov 17;16(12):1180–91.

56. Carlson BA, Tobe R, Yefremova E, Tsuji PA, Hoffmann VJ, Schweizer U, et al. Glutathione peroxidase 4 and vitamin E cooperatively prevent hepatocellular degeneration. Redox Biol. 2016 Oct;9:22–31.

57. Yang WS, Stockwell BR. Ferroptosis: Death by Lipid Peroxidation. Trends Cell Biol. 2016 Mar;26(3):165–76.

58. Dickinson DA, Forman HJ. Cellular glutathione and thiols metabolism. Biochem Pharmacol. 2002;64(5):1019–26.

59. Marengo B, De Ciucis C, Verzola D, Pistoia V, Raffaghello L, Patriarca S, et al. Mechanisms of BSO (L-buthionine-S,R-sulfoximine)-induced cytotoxic effects in neuroblastoma. Free Radic Biol Med. 2008 Feb;44(3):474–82.

60. Yang WS, Stockwell BR. Synthetic Lethal Screening Identifies Compounds Activating Iron-Dependent, Nonapoptotic Cell Death in Oncogenic-RAS-Harboring Cancer Cells. Chem Biol. 2008 Mar;15(3):234–45.

61. Dixon SJ, Patel DN, Welsch ME, Skouta R, Lee ED, Hayano M, et al. Pharmacological inhibition of cystine–glutamate exchange induces endoplasmic reticulum stress and ferroptosis. eLIFE. 2014;

62. Murphy TH, Miyamoto M, Sastre A, Schnaar RL, Coyle JT. Glutamate toxicity in a neuronal cell line involves inhibition of cystine transport leading to oxidative stress. Neuron. 1989;1547–58.

63. Conrad M, Sato H. The oxidative stress-inducible cystine/glutamate antiporter, system x c − : cystine supplier and beyond. Amino Acids. 2012 Jan;42(1):231–46.

64. Sato H, Tamba M, Ishii T, Bannai S. Cloning and expression of a plasma membrane cystine/glutamate exchange transporter composed of two distinct proteins. J Biol Chem. 1999;274(17):11455–8.

65. Yang WS, SriRamaratnam R, Welsch ME, Shimada K, Skouta R, Viswanathan VS, et al. Regulation of Ferroptotic Cancer Cell Death by GPX4. Cell. 2014 Jan;156(1-2):317–31.

66. Yang WS, Kim KJ, Gaschler MM, Patel M, Shchepinov MS, Stockwell BR. Peroxidation of polyunsaturated fatty acids by lipoxygenases drives ferroptosis. Proc Natl Acad Sci. 2016 Aug 23;113(34):E4966–75.

67. Dixon SJ, Winter GE, Musavi LS, Lee ED, Snijder B, Rebsamen M, et al. Human Haploid Cell Genetics Reveals Roles for Lipid Metabolism Genes in Nonapoptotic Cell Death. ACS Chem Biol. 2015 Jul 17;10(7):1604–9.

68. Shimada K, Rachid S, Kaplan A, Yang WS, Hayano M, Dixon SJ, et al. Global survey of cell death mechanisms reveals metabolic regulation of ferroptosis. Nature chemical biology. 2016;497–503.

69. Huang H-S, Chen C-J, Lu HS, Chang W-C. Identification of a lipoxygenase inhibitor in A431 cells as a phospholipid hydroperoxide glutathione peroxidase. FEBS LETT. 424th ed. 1998;22–6.

70. Imai H, Narashima K, Arai M, Sakamoto H, Chiba N, Nakagawa Y. Suppression of leukotriene formation in RBL-2H3 cells that overexpressed

phospholipid hydroperoxide glutathione peroxidase. J Biol Chem. 1998;273(4):1990–7.

71. Schneider M, Wortmann M, Mandal PK, Arpornchayanon W, Jannasch K, Alves F, et al. Absence of Glutathione Peroxidase 4 Affects Tumor Angiogenesis through Increased 12/15-Lipoxygenase Activity. Neoplasia. 2010 Mar;12(3):254–63.

72. Agbor TA, Demma Z, Mrsny RJ, Castillo A, Boll EJ, McCormick BA. The oxido-reductase enzyme glutathione peroxidase 4 (GPX4) governs *S almonella* Typhimurium-induced neutrophil transepithelial migration: GPX4 and PMN transmigration in *S* . Typhimurium infection. Cell Microbiol. 2014 Sep;16(9):1339–53.

73. Persaud A, Alberts P, Amsen EM, Xiong X, Wasmuth J, Saadon Z, et al. Comparison of substrate specificity of the ubiquitin ligases Nedd4 and Nedd4-2 using proteome arrays. Mol Syst Biol [Internet]. 2009 Dec 1 [cited 2016 Sep 19];5. Available from: http://msb.embopress.org/cgi/doi/10.1038/msb.2009.85

74. Roveri A, Maiorino M, Nisii C, Ursini F. Purification and characterization of phospholipid hydroperoxide glutathione peroxidase from rat testis mitochondrial membranes. Biochim Biophys Acta. 1994;211–21.

75. Bensadoun A, Weinstein D. Assay of proteins in the presence of interfering materials. Anal Biochemistry. 1976;241–50.

76. Tietze F. Enzymatic method for quantitative determination of nanogram amounts of total and oxidid glutathione: application to mammalian blood and other tissue. Analytical Biohemistry. 1969;502–22.

77. Boase NA, Kumar S. NEDD4: The founding member of a family of ubiquitin-protein ligases. Gene. 2015 Feb;557(2):113–22.

78. Griffith OW, Meister A. Potent and specific inhibition of glutathione synthesis by buthionine sulfoximine (S-n-butyl homocysteine sulfoximine). J Biol Chem. 1979;7558–60.

79. Bannai S. Induction of Cystine and Glutamate Transport Activity in Human Fibroblasts by Diethyl Maleate and Other Electrophilic Agents. The journal of Biological Chemistry. 4th ed. 1984;2435–40.

80. Rampersad SN. Multiple Applications of Alamar Blue as an Indicator of Metabolic Function and Cellular Health in Cell Viability Bioassays. Sensors. 2012 Sep 10;12(12):12347–60.

81. Friedmann Angeli JP, Schneider M, Proneth B, Tyurina YY, Tyurin VA, Hammond VJ, et al. Inactivation of the ferroptosis regulator Gpx4 triggers acute renal failure in mice. Nat Cell Biol. 2014 Nov 17;16(12):1180–91.

82. Carlson BA, Tobe R, Yefremova E, Tsuji PA, Hoffmann VJ, Schweizer U, et al. Glutathione peroxidase 4 and vitamin E cooperatively prevent hepatocellular degeneration. Redox Biol. 2016 Oct;9:22–31.

83. Sengupta A, Lichti UF, Carlson BA, Cataisson C, Ryscavage AO, Mikulec C. Targeted disruption of glutathione peroxidase 4 in mouse skin epithelial cells impair postnatal hair follicle morphogenesis that is partially rescued through inhibition of COX-2. JInvest Dermatol. 133rd ed. 2013;1731–41.

84. Persaud A, Rotin D. Use of proteome arrays to globally identify substrates for E3 ubiquitin ligases. Methods Mol Biol. 759th ed. :215–24.

85. Song X, Xie Y, Kang R, Hou W, Sun X, Epperly MW. FANCD2 protects against bone marrow injury from ferroptosis. Biochem Biophys Res Commun. 2016;

86. Rieser E, Cordier SM, Walczak H. Linear ubiquitination: a newly discovered regulator of cell signalling. Trends Biochem Sci. 2013 Feb;38(2):94–102.

87. Xu P, Duong DM, Seyfried NT, Cheng D, Xie Y, Robert J, et al. Quantitative Proteomics Reveals the Function of Unconventional Ubiquitin Chains in Proteasomal Degradation. Cell. 2009 Apr;137(1):133–45.

88. Ball KA, Johnson JR, Lewinski MK, Guatelli J, Verschueren E, Krogan NJ, et al. Non-degradative Ubiquitination of Protein Kinases. PLoS Comput Biol. 2016;12(6):e1004898.

89. Chen ZJ, Sun LJ. Nonproteolytic Functions of Ubiquitin in Cell Signaling. Mol Cell. 2009 Feb;33(3):275–86.